Global metabolomics and lipidomics approaches to probe virus-host interactions

Zhang, Z.

Chapter 4

Development of a targeted HILIC-MS/MS based lipidomics platform applied to a coronavirus disease severity study

Based on

Zhengzheng Zhang*, Madhulika Singh*, Alida Kindt, Agnieszka B. Wegrzyn, Mackenzie J. Pearson, Ahmed Ali, Amy C. Harms, Paul Baker, Thomas Hankemeier

Plasma Development of a targeted hydrophilic interaction liquid chromatography-tandem mass spectrometry based lipidomics platform applied to a coronavirus disease severity study

J Chromatogr A .31 august 2023; 1708: 464342.

*Authors contributed equally

Abstract

The importance of lipids seen in studies of metabolism, cancer, the recent COVID-19 pandemic and other diseases has brought the field of lipidomics to the forefront of clinical research. Quantitative and comprehensive analysis is required to understand biological interactions among lipid species. However, lipidomic analysis is often challenging due to the various compositional structures, diverse physicochemical properties, and wide dynamic range of concentrations of lipids in biological systems. To study the comprehensive lipidome, a hydrophilic interaction liquid chromatography-tandem mass spectrometry (HILIC-MS/MS)-based screening method with 1200 lipid features across 19 (sub)classes, including both nonpolar and polar lipids, has been developed. HILIC-MS/MS was selected due to its class separation property and fatty acyl chain level information. 3D models of class chromatographic retention behavior were established and evaluations of cross-class and within-class interferences were performed to avoid over-reporting these features. This targeted HILIC-MS/MS method was fully validated, with acceptable analytical parameters in terms of linearity, precision, reproducibility, and recovery. The accurate quantitation of 608 lipid species in the SRM 1950 NIST plasma was achieved using multi-internal standards per class and post-hoc correction, extending current databases by providing lipid concentrations resolved at fatty acyl chain level. The overall correlation coefficients (R2) of measured concentrations with values from literature range from 0.64 to 0.84. The applicability of the developed targeted lipidomics method was demonstrated by discovering 520 differential lipid features related to COVID-19 severity. This high coverage and targeted approach will aid in future investigations of the lipidome in various disease contexts.

Keywords: HILIC-MS/MS; Clinical lipidomics; Quantitation; NIST SRM 1950 plasma; COVID-19; Over-reporting

1. Introduction

Lipids play a critical role in defining cellular and sub-cellular structures, signaling, modifying metabolic processes and energy storage [1]. Imbalance of lipids in the body (dyslipidemia) has been linked to multiple disorders such as neurodegenerative diseases [2], cancer [3], metabolic syndrome [4], and dysregulation of the gut microbiome [5]. The role of lipids also showed an important role in the individuals affected by the recent pandemic caused by coronavirus (COVID-19). Several lipidomic investigations have documented a modified lipidome profile in individuals affected by COVID-19 [6–13]. In an initial study conducted during the pandemic by Shen et al., patients with varying degrees of COVID-19 severity exhibited reduced levels of sphingolipids, and glycerophospholipids in their serum, while phosphatidylcholine (PC) levels were increased [6]. Another study found decreased plasma diglycerides (DG) and elevated levels of sphingomyelins (SM) in COVID-19 patients [12]. Other studies have indicated decreased serum levels of total cholesterol, HDL, and LDL, with increased levels of triglycerides (TG) [13]. These findings suggest an overall disruption in lipid metabolism in COVID-19, highlighting how lipidomics is essential in understanding the role played by lipids in disease progression, and for developing prevention strategies in translational clinical studies.

Deciphering the interplay between the lipidome and other parts of the biological system requires a deep understanding of the complex pathways of lipid metabolism, the function of lipids, and how lipids are generated and interact with other molecules. This can only be achieved by analytical methods with exhaustive coverage and good quantitative performance. Consequently, two major challenges must be addressed by lipidomics methods: 1) elucidating the diverse compositional structures of lipids in detail, and 2) quantifying the biological concentrations of lipids over a wide dynamic range [14]. Mass spectrometry (MS)-based lipidomics methodologies can be divided into two groups, species-separation based and class-separation based, irrespective of their separation mechanisms. The class-based separations, like differential ion mobility, hydrophilic interaction chromatography (HILIC) [15,16], normal-phase liquid chromatography (NPLC) [17], and supercritical fluid chromatography (SFC), are powerful in resolving the isobars. These techniques also facilitate the co-elution of lipid species and their internal standards (ISs) for accurate quantification. Species-separation based techniques like reverse phase

liquid chromatography (RPLC) and trapped ion-mobility have limitations in achieving reliable quantitation, as ISs often do not co-elute with analytes and suffer from cross-class isobaric interference [18,19]. Multiple reaction monitoring (MRM) is frequently selected as the MS method due to its high sensitivity and additional acyl tail characterization of phospholipid species [20]. The combination of separation techniques, such as HILIC, ion mobility, with MRM are often being used in large scale targeted lipidome profiling [21–25]. Direct infusion methods with or without ion mobility may encounter severe matrix effect, consume large amount samples, exhibit lower sensitivity and have limitation in the separation of isomers/isobars [22]. Another important aspect in the lipidomics study is the unambiguous identification of lipid species, as there are several sources of cross-class interference (isobars/isomers, in-source fragments) and within-class interference (isotopes and different ion types), which can lead to over-reporting of lipid species [26].

Achieving absolute quantitation is another challenge in lipidomics due to commercial unavailability of (internal) standards for all endogenous lipid species. Recognizing the difficulties in achieving absolute quantitation, we refer to all attempts to report data in molar concentrations as accurate quantitation. These efforts include using multiple internal standards with different chain length and double bond numbers per class and, or applying response correction factors for quantification [27,28]. Although it must be noted that true accurate quantification would require the systematic use of individual standards per species, a standardized analytical workflow with unambiguous identification resolving the complexity associated with lipidomics analysis can ensure highly reliable data that can also be correlated with other studies [29,30].

The comprehensive coverage of the lipidome is necessary for biomarker discovery and pathway mapping. HILIC-MS/MS is chosen in this study for large-scale metabolic profiling because of its superior quantitative performance due to close elution of ISs and corresponding lipid molecular species, thus diminishing differential matrix effects. The experimental design in this paper aims to screen lipid species to minimize over-reporting and enhancing confidence in lipid identification. This HILIC-MS/MS method targets 19 lipid (sub)classes in a 14 min analytical run. Firstly, a MS/MS library was built for routine lipid screening followed by assigning lipid identification confidence scores after evaluation of various cross-class and within-class interference correction. The method validation was

performed according to the bioanalytical method validation guidelines as precisely as possible. The accurate quantitation was conducted using multiple internal standards per class and was performed on National Institute of Standards and Technology Standard Reference Material 1950 (NIST SRM 1950) plasma for lipid species with high confidence score. As a proof of applicability, the developed HILIC-MS/MS lipidomics method was used to characterize the lipidome of plasma samples from coronavirus disease 2019 (COVID-19) patients. The results showed a wide class-based changed lipidome correlated with disease severity, indicating the potential for disease progression prediction using lipidomics.

2. Experimental section

2.1. Reagent and Materials

Acetonitrile, methanol (LC-MS grade), and chloroform (HPLC grade) were purchased from Biosolve Chimie (Dieuze, France). LiChropur™ quality ammonium acetate was purchased from Merck KGaA (Darmstadt, Germany). Water was purified by Milli-Q® reference water purification system purchased from Merck KGaA (Darmstadt, Germany). Two lipid standards from each class were used for HILIC-MS/MS method development. The standard mix for method development consists of the system suitability kit for the Lipidyzer platform (part no.5040407) purchased from AB Sciex (Framinghan MA, USA) and it includes ceramides (Cer), cholesterol esters (CE); diglycerides (DG); lysophosphatidylcholine (LPC); lysophosphatidylethanolamine (LPE); phosphatidylcholine (PC); phosphatidylethanolamine (PE); sphingomyelin (SM); triglycerides (TG); hexosylceramides (HexCer); lactosylceramdides (LacCer). Individual standards such as galactosyl ceramide, GalCer 18:1;O2/16:0; glucosyl ceramide GluCer 18:1;O2/16:0; phosphatidylglycerol, PG 14:0/14:0 and PG 17:0/17:0; Bis(Monoacylglycero) Phosphate, BMP 14:0/14:0 and BMP 18:1/18:1; phosphatidylserines, PS 14:0/14:0 and PS 16:0/16:0; phosphatidylinositols, PI 18:0/20:4 and PI 16:0/18:1; lysophosphatidylglycerol, LPG 17:1 and LPG 18:1; lysophosphatidylinositol, LPI 17:1 and LPI 20:4; lysophosphatidylserines, LPS 17:1 and LPS 18:1 were purchased from Avanti Polar Lipids (Alabaster, AL, USA).

The one-IS per class mix was used for the validation of the method and application in the

COVID-19 plasma samples, consisting of SPLASH® LIPIDOMIX® Mass Spec Standard (330707-1EA), LPS 17:1; LPI 17:1; LPG 17:1 purchased from Avanti polar lipids and deuterated hexosylceramides (Hex-Cer 18:1;O2/16:0-d9) (part no.5040398), deuterated lactosylceramide (Lac-Cer 18:1;O2/16:0-d9) (part no.5040399), deuterated dihydroceramide (Cer 18:0;O2/16:0-d9) (part no.5040397), deuterated ceramides (Cer 18:1;O2/16:0-d9) (part no.5040167) purchased from AB Sciex. The one-IS per class mix were also spiked in the COVID-19 samples as internal standard (as shown in **Supplemental Table S1**).

The multi-ISs per class mix was used for accurate quantitation, consisting of UltimateSPLASH™ ONE (330820L-1EA), SPLASH® LIPIDOMIX® Mass Spec Standard (330707-1EA), LPS 17:1, LPI 17:1, LPG 17:1 purchased from Avanti Polar lipids; Hex-Cer 18:1;O2/16:0-d9 (part no.5040398), Lac-Cer 18:1;O2/16:0-d9 (part no.5040399), Cer 18:0;O2/16:0-d9 (part no.5040397) purchased from AB Sciex were used for quantitation (as shown in **Supplemental Table S2**). All stock solutions, standards and calibration solutions were prepared in acetonitrile-methanol mixture (3:7 v/v).

2.2. Plasma sample collection

Human K2 Ethylenediaminetetraacetic acid (EDTA) plasma was purchased from Innovative research (Novi, MI, USA) and used for method development and validation. NIST SRM 1950 human plasma for quantitation was purchased from Avanti Polar Lipids (Alabaster, AL, USA).

The COVID-19 cohort consisted of 44 adults admitted to the regional Amphia hospital in Breda, the Netherlands, on 24 March 2020–14 April 2020, as published earlier [31,32]. **Supplemental Table S3** summarizes key characteristics of the 44 patients and 103 collected plasma samples. EDTA plasma samples were collected in intervals of 3–4 days throughout the study. All patients reported COVID-19 related complaints, tested positive for the SARS-CoV-2 by polymerase chain reaction (PCR), and gave consent to be included in the study. The study was performed in accordance with the guidelines for sharing of patient data of observational scientific research in case of exceptional health situations.

2.3. Sample preparation

Lipids were extracted from 25 uL of plasma (human K2 EDTA plasma/ COVID-19 patient plasma) according to the methyl tert-butyl ether (MTBE) method [33]. A volume of 34 µL of the one-IS per class mix was added to 25 µL of plasma and vortexed. To this mixture, 231 µL of methanol (MeOH) and 770 µL of MTBE were added. The sample was incubated at room temperature on an orbital shaker for one hour followed by the addition of 192.5 µL of water thus making final ratio MTBE:MeOH:Water (10:3:2.5, v/v/v). The mixture was again incubated at room temperature for 10 min and then centrifuged at 15,800 rcf for 10 min. A volume of 520 µL of upper layer was collected and dried in a vacuum concentrator followed by reconstitution in 200 µL of acetonitrile:methanol (3:7). This mixture was vortexed and centrifuged for 10 min. The supernatant was collected and injected in the LC–MS for analysis.

The COVID-19 study batch design includes solvent blanks, procedure blanks (with IS), clinical study samples and quality control (QC) samples. These QC samples were a pool of all the study plasma samples and were analyzed at regular intervals in the study batch to determine the performance of the method.

2.4. Lipidomics profiling analysis

A QTRAP 6500+ (AB Sciex, Concord, ON, Canada) coupled to an Exion LC AD (AB Sciex, Concord, ON, Canada) was used for targeted lipid profiling to obtain lipid information including retention time (t_R) and MS/MS fragments. The column used for the separation was a Luna amino column (100 mm × 2 mm, 3 µm, Phenomenex). The mobile phase A was 1 mM ammonium acetate in chloroform: acetonitrile (1:9), while mobile phase B was 1 mM ammonium acetate in acetonitrile: water (1:1). The gradient is shown in Supplemental Table S4, A. Two injections were made to accommodate all the MRM transitions of the targeted lipid features. The injection volume was 5 µL for the first acquisition run and 1 µL for the second acquisition run. The column temperature was kept at 35 ◦C. The injector needle was washed with isopropanol:water: dichloromethane (94:5:1, v/v/v) after each injection.

MS/MS experiments were done on QTRAP 6500+ mass spectrometer with a Turbo V source (AB Sciex, Concord, ON, Canada) operated with electrospray ionization (ESI) probe. The

declustering potential (DP) and collision energy (CE) of lipid transitions were optimized to obtain the highest response for the mixture of lipid standards. The information about the precursor ion (Q1), characteristic product ion (Q3), lipid name (ID), optimized DP, and CE of all the lipid features were incorporated into the MS acquisition method before the screening in plasma samples. The parameters of the QTRAP 6500+ mass spectrometer were as follows: curtain gas (N2) was 20 psi; collision gas (N2) kept at medium, ion spray voltage was 5500 V and -4500 V for positive and negative mode respectively; source temperature was 400 ◦C, GS1 and GS2 were 30 and 35 psi respectively. Scheduled MRM (sMRM) was used for data acquisition for targeted analysis. sMRM window, ion transitions and t_R are summarized in supplementary info (**Supplemental Table S5, sheet 1 and 2**). The total scan time was 0.5 s. The lipids detected by the UHPLCQTRAP based lipidomics profiling analysis were processed using AB Sciex OS (version 2.1.6, AB SCIEX, Concord, ON, Canada).

The method for accurate mass measurements was based on the previously reported RPLC-HRMS method [34]. An Acquity UPLC (Waters, Milford, MA, USA) was coupled to a SCIEX ZenoTOF 7600 system (Darmstadt, Germany). The column used was Waters Acquity HSS T3 column (2.1 × 100 mm, 1.8 µm, Waters, Milford, MA). The mobile phase A was 10 mM ammonium formate in acetonitrile: water (6:4), while mobile phase B was 10 mM ammonium formate in isopropanol: acetonitrile (9:1). This gradient is described in Supplemental Table S4, B. The following ion source parameters were used: ESI spray voltage was 5.2 Kv and 4.5 kV in the positive and negative ionization mode respectively, a capillary temperature of 550 ◦C, ion source gas 1 50 psi, ion source gas 2 50 psi, curtain gas of 35 psi, and CAD gas of 7 psi. A survey TOFMS scan was performed in the mass range of (300–1000) Da in Information Dependent Acquisition mode (IDA).

2.5. Method validation

The one-IS per class mix (specified in reagents and material section) has been used to calculate the various validation parameters. An 8-point calibration line (cal-1 to cal-8) was made by serial dilution of IS present in the one-IS per class mix to determine the linear range. The concentrations of these calibration points are mentioned in the supplementary information (**Supplemental Table S6**). The serially diluted standards of the one-IS per class

mix were spiked in three different ways to prepare the calibration curves: a) in pure solvent (without matrix), b) spiking the standard in human K2 EDTA plasma before following the extraction described in the sample preparation section, c) spiking the standard in human K2 EDTA plasma after extraction. The calibration curves were prepared on three different days using freshly prepared standards. To determine the linear range, we used an unweighted linear regression model. The determination of various validation parameters was performed by spiking one-IS per class mix at low (L), medium (M) and high (H) concentration levels. Low levels (L) were chosen to be 3 times higher than the lower limit of quantitation (LLOQ). Medium levels (M) were set to be around 30–50% of the calibration range. The high level (H) samples were spiked at close to 75% of the upper limit of quantitation (ULOQ). The details about the calculations of validation parameters such as carryover, precision, ion suppression and matrix effects are described in **supplementary information**. The limit of detection (LOD) and limit of quantification (LOQ) were calculated based on the signal-to-noise ratio of 3 and 10 respectively. The equations used for the calculations of LOD and LOQ are described in supplementary information. The repeatability was evaluated to assess any deviation in analysis over time and is an important criteria to assess the performance of the method when running longer batches. We evaluated the repeatability of our method by calculating relative standard deviation (RSD %) of endogenous lipid features in QC samples of COVID-19 patients. In this work, the lipid species with RSD below 15% in QC samples were classified as high confidence metabolites while those in the range of (15–30)% were treated with caution (as shown in **Supplemental Table S5, sheet 7**). Since we are doing exploratory study, we considered metabolites with RSD up to 30% to accommodate variations due to class behavior.

2.6. Accurate quantitation in the NIST SRM 1950 plasma

NIST SRM 1950 plasma samples were used for the accurate quantitation of endogenous lipid species. Six-point calibration lines were prepared by serially diluting the multi-ISs per class mix. These six points were spiked in NIST SRM 1950 plasma samples before extraction and lipid extraction was performed according to the protocol specified in **Section 2.3**. The details of the initial concentration of multi-ISs mix internal standards are specified in supplementary information (**Supplemental Table S2**). The concentrations of these calibration lines (cal-1 to cal-6) are mentioned in supplementary information

(**Supplemental Table S5, sheet 5**).

To estimate the concentrations of endogenous compounds in human plasma, an unweighted linear regression model (y = ax + b, where x represents the metabolite concentration) was used, based on the calibration curves. The model fitness was estimated using R2. Where intercept 'b' was not significant ($p > 0.05$) for the model fit, the intercept was set to 0 (y = ax + 0). The lipid concentrations were calculated in nmol mL^{-1} to compare with other reported studies. Type II isotopic correction was performed using LICAR [35]. The concentration calculation of the species with same fatty acyl chain will be influenced by the selection of MRM transition used for IS, as the response of sn-1 and sn-2 chains is different as shown in **Supplemental Table S9**. Post-hoc correction was used to correct for the metabolites with two same fatty acyl chains to remove the double signal.

2.7. Data processing and statistical analysis

A model establishing a relation between t_R and the length of fatty acyl chains (carbon number, CN) as well as the number of double bond equivalents (DBEs) was generated for each lipid class using multivariate analysis. The models with error rates higher than 20% or $R2 < 0.9$ were treated with caution.

A linear regression model was used to find the most important biomarker candidates distinguishing the patients at ward from intensive care unit (ICU). All variables were cuberoot-transformed prior to statistical analyses. Differential analysis between ICU and ward patients incorporating all samples was performed using linear regression correcting for age, sex, and BMI, grouped by patient, and weighted by the inverse number of observations per patient. The p-values obtained in all tests were adjusted for multiple testing using the Benjamini–Hochberg method implemented in the p.adjust R function (v.4.0.3), and termed Qvalues. The statistical significance was set at $Q < 0.05$ to determine the lipid biomarkers related to COVID-19 disease severity between ICU patients and ward patients. Principal component analysis (PCA) and volcano plot visualization were conducted. All statistical analyses were performed in R (version 4.0.3), and graphs were plotted using the packages ggpubr and stats.

3. Results and discussion

The aim of the present study is to establish the HILIC-MS/MS based targeted lipidomics method with high coverage that can be used for comprehensive profiling and quantification of the plasma lipidome.

3.1 Construction of the lipid database

MRM transitions were split into two methods in polarity switching mode, depending on the biological concentration of the lipid classes. The first and second acquisition methods contained 602 and 598 ion pairs, respectively. The complete list is shown in **Supplemental Table S5 (sheets 1 and 2)**. A total of 19 lipid subclasses could be summarized as DG, TG, CE, PC, PE, alkyl and alkenyl substituent PEs (PE-O) & (PE-P), PG, PS, PI, LPC, LPE, LPS, LPI, LPG, Cer, HexCer, LacCer and SM. The lipid naming convention used will follow the guidelines established by Liebisch et al. [36] and additionally, by the Lipid Maps Consortium. The complete lipid identifiers (Lipidmaps, Swisslipids, MetaNetX, CHEBI, PubChem, HMDB, LipidX, InChI and InChI key) are listed in **Supplemental Table S5, sheet 3**. All classes of phospholipids and lysophospholipids were measured in the negative mode as it enabled the identification of fragment ions corresponding to the fatty acyl chains (not positional information), e.g., PC 18:1_18:2. The phospholipids are analyzed using one fatty acyl chain, as the second chain can be characterized by measuring the total carbon count and subtracting the measured chain. The MRM transitions of TG and DG are generated using neutral loss of one fatty acyl tail in positive mode. Only one tail has been reported for TG, e.g. TG 16:1_51:2, where 16:1 will be one of the fatty acyl chain out of three chain in TG 51:2.

Five criteria were used for the confirmation of identification for all lipid features: **Class separation and cross-class interference**, Criteria1: lipid features detected in the HILIC-MS/MS method; Criteria 2: lipid class chromatographically separated or has a diagnostic fragment in the case of overlapping chromatographic peaks; **Within-class separation and interference**, Criteria 3: lipid features confirmed by accurate mass using RPLC-HRMS; Criteria 4: lipid features with full chromatographic separation; Criteria 5: lipid features matched with retention time model; Criteria 6: lipid features showing non-zero

concentration after isotopic and interfering adduct/ion type correction. The confidence of lipid identification will be indicated using confidence level scores, score 4 being the highest while score 1 the lowest. An overview of the lipid identification workflow and confidence level score is shown in **Fig. 1(A) and (B**).

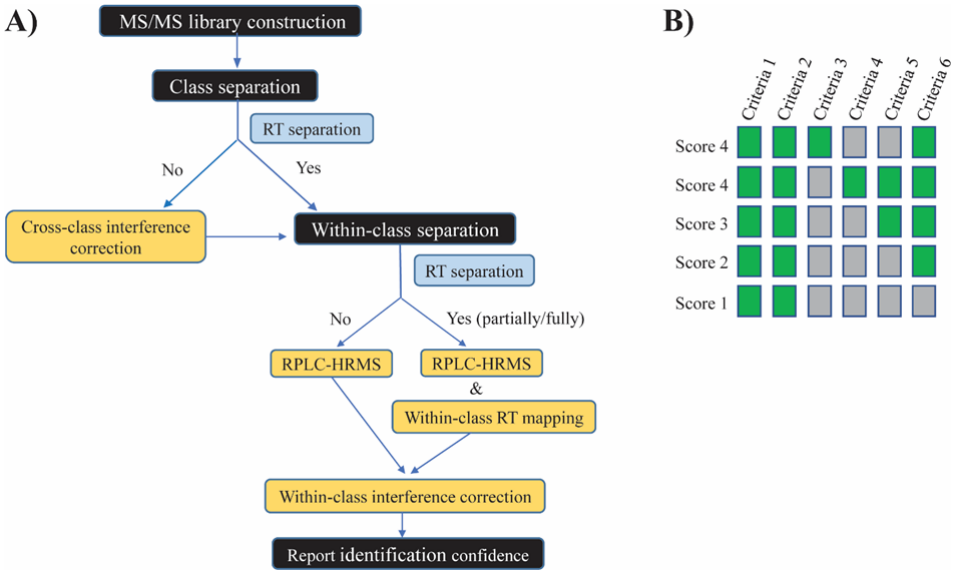

Fig. 1. (A) Decision tree of lipids identification; (B) score levels of identification confidence. Criteria 1: lipid features detected in the HILIC-MS/MS method; Criteria 2: lipid class chromatographically separated or has a diagnostic fragment in the case of overlapping chromatographic peaks; Criteria 3: lipid features confirmed by accurate mass using RPLC-HRMS; Criteria 4: lipid features with full chromatographic separation; Criteria 5: lipid features matched with retention time model; Criteria 6: lipid features showing non-zero concentration after isotopic and interfering adduct/ion type correction. The green boxes represent the fulfillment of the criteria. RT-Retention time; RPLC-HRMS- Reverse phase liquid chromatography-high resolution mass spectrometry.

3.2 Class separation and cross-class interference of lipids in the HILICMS/MS method

The UHPLC system coupled to the QTRAP 6500+ mass spectrometer was employed for targeted acquisition of lipids in MRM XIC chromatograms of standards spiked in plasma are shown in **Fig. 2(A).** The class retention time was confirmed by 3–5 standards per class with different chain length and carbon number. In HILIC chromatography, individual lipid classes are separated according to polarity of the head group. Therefore, the non-polar

character of TG, DG and CE leads to the least retention for these classes, followed by Cer at the beginning of the chromatogram. The more polar lipid classes, such as PC, PE, PG, PI, HexCer, LacCer, SM, LPC, LPE, LPG elute over a wide t_R range in the middle part of the chromatogram. The most polar lipids PS, LPI and LPS elute at the end of the chromatogram. The first step (criteria 1) of the identification involves the detection of the lipid features in the HILICMS/MS method. The limit of detection (LOD) was first determined for each class, and features that were detected over the LOD threshold were further checked for interference from background signal. The repeatability of six replicates of the same plasma samples were examined, and the features with deviation above 30% in these replicates were excluded.

The next step (criteria 2) of identification was the evaluation of cross-class interferences. The classes should either be chromatographically separated or should have a diagnostic fragment for clear identification. GalCer and GluCer are an example of isomeric interferences that do not separate chromatographically and co-elute and hence, they are reported as HexCer. PG and BMP are another example of isomeric lipid classes which are chromatographically well-separated as seen in the standards in **Fig. 2(A)** (the coverage of endogenous BMPs can be extended in the future). SM has been reported to have isobaric interference from PC as they generate the same product ion 184.1 from their headgroup in the positive ion mode, but this interference can be resolved as these two classes are separated by retention time.

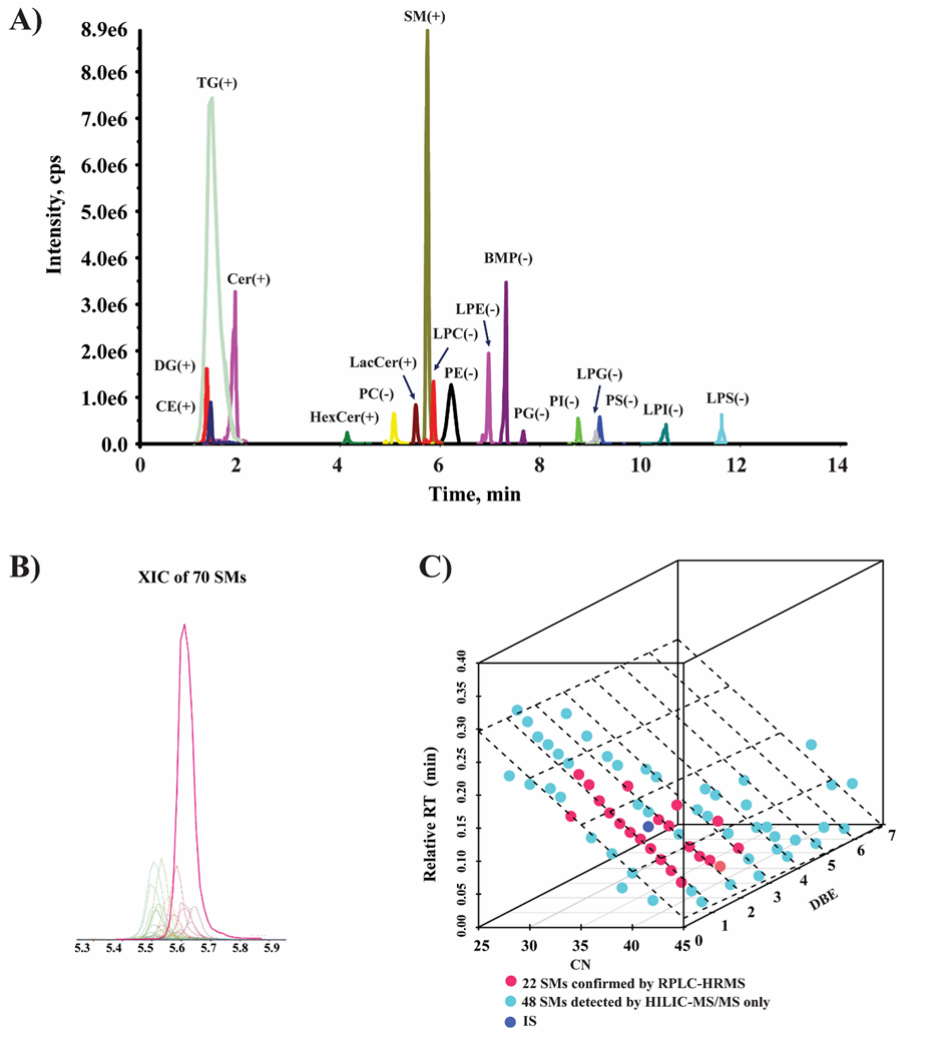

Fig. 2. A) Representative XIC chromatograms of standards spiked in plasma by HILIC-MS/MS lipidomics analyses in switching polarity modes (positive (+) and negative (-)). B) XIC chromatograms of 70 SMs detected in plasma using HILIC-MS/MS method. C) 3D model for retention time mapping with carbon number (CN) and for 70 SMs detected by the HILIC-MS/MS method. 22 SMs confirmed by RPLC-HRMS are colored in red, the remaining SMs fitting the retention time model with error rates less than 20% are colored in light blue and SM 18:1;O2/18:1-d9(IS) is in dark blue. Peak annotation: TG- Triglyceride; DG- Diglyceride; CE- Cholesteryl ester; Cer- Ceramide; HexCer - Hexosyl ceramide; PC - Phosphatidylcholine; LacCer- Lactosyl ceramide; SM- Sphingomyelin; LPC- Lysophosphatidylcholine; PE-Phosphatidylethanolamine; LPE- Lysophosphatidylethanolamine; BMP- Bis(Monoacylglycero)Phosphate; PG- Phosphatidylglycerol ; PI- Phosphatidylinositol; LPG- Lysophosphatidylglycerol; PS- Phosphatidylserine; LPI- Lysophosphatidylinositol; LPS- Lysophosphatidylserine.

There are also potential cross-class interferences due to in-source fragmentation. PC undergoes in-source fragmentation to generate PE in negative ionization mode [37]. Lysophospholipids and phospholipids will generate ions from their fatty acyl chains that can be misannotated as free fatty acids (FFAs) or they can also lose their head group and misannotated as lysophosphatidic acid (LPA) or phosphatidic acid (PA). In positive mode, glycosphingolipids could lose their head group,

generating respective ceramide fragment [38]. But all of these potential cases of interferences due to in-source fragmentation are well separated by the chromatography. TG is a common in-source fragmentation source for DG, however ammonium adducts of TG in positive polarity mode undergoes neutral m/z loss of NH3 and a fatty acid chain [39]. After the neutral loss, the remaining part of TG corresponds to the in-source fragment of DG [M + H]$^+$ (protonated form) instead of DG [M + NH4]+. Since the ammonium adduct of DG is used in our method for analysis, the problem with TG's in-source fragmentation is avoided.

After cross-class interference screening, the lipid features will be evaluated for within-class interference.

3.3 Within-class separation and interference of lipid features in HILICMS/MS method

The further identification (criteria 3) of lipid features from the HILICMS/MS method library was performed by their accurate mass determination by RPLC-HRMS method as reverse phase has superior performance in within-class species separation. Apart from accurate mass determination, the fatty acyl chain information was also checked for classes TG, DG, PC, PE and PI by using IDA mode (**Supplemental Table S5, sheet 3**).

The next step for the identification of lipid features was through chromatographic t_R in the HILIC-MS/MS method, which is a very important parameter for lipid identification. The individual lipid features within class are separated according to the carbon number and the double bond equivalents. The lipid features in the classes LPC, LPE, LPG, SM, PI, PS, PE and PC are partially separated and elute over a range of t_R (0.2–0.4) min while features with different acyl chains in the classes LPI and LPS are fully separated and elute over a retention time range of 0.7 min and 1.13 min, respectively (**Supplemental Table S7**). The lipid features belonging to the classes TG, DG, CE, Cer, HexCer, LacCer and PG, show no

separation and elute at a range spanning less than 0.05 min. Criteria 4 was assigned to the features belonging to the fully separated classes.

A)

B)

Compound name	Interference	Ion type	Instrument type	Precursor Ion	Product Ion	Correction required
*SM 40:4;O2		[M+H]+		781.6218	184	
	SM 41:2;O2	[M+H-H2O]+	HILIC-HRMS	781.6582	n/a	NO
		[M+H-H2O]+	HILIC-MS/MS	781.7	184	**YES**
	SM 38:1;O2	[M+Na]+	HILIC-HRMS	781.6194	n/a	**YES**
		[M+Na]+	HILIC-MS/MS	781.6	206	NO
		[M+Na]+	HILIC-MS/MS	781.6	184	**YES**

Fig. 3. A) An example of XICs of monoisotopic peaks of three SMs and structure of different ion type ($+H^+$, $+Na^+$, $-H_2O$) of SM in positive mode. B) The possible interference from different ion types of SM in HILIC- HRMS and MRM analysis.
** putatively annotated SM with score 2*

Further, retention time models were built for partially/fully separated classes to match retention pattern with lipid features (criteria 5). To study the retention behavior of lipid features within each class in HILIC, relative dependencies of t_R on the CN and the DB number are fitted using a multiple linear regression model using the unambiguously identified lipid features. As seen in **Fig. 2(B) and (C)**, SM features are separated over a range of 0.31 min. In **Supplemental Table S5 (sheet 3)**, out of the 71 SM features, 70 features detected in the HILIC method and 22 SM features unambiguously identified using RPLC-HRMS were utilized to create a 3D model. In total, 70 SMs fit in the model with error rates of 11.9% and an R2 of 0.97 after removal of the outliers with error rates higher than 20% or R2 < 0.9 (Fig. 2(C)). The PS class had higher error rates (23.94%) due to fewer number of features (data not shown). In general, the higher carbon number in fatty acyl

chains corresponds to decreased t_R in HILIC (Fig. S1). Double bond equivalents contribute little in the separation of different lipid features in SM, PC, PE classes and result in partial or full separation in the t_R of LPC, LPE, PI, LPG, PS, LPI, LPS.

All detected features with no/partial separation went through the quantifying corrections for different ion types and isotopes. We will take an example of SM for illustration of ion type interference. The primary observed ion types generated in positive mode for SMs are $[M + H]^+$, [M + Na]+, and $[M + H - H_2O]^+$, with $[M + H]^+$ being the most intense peak. If we consider SM 40:4;O2, the primary ion type interference for $[M+H]^+$ could be caused by $[M + Na]^+$ of SM 38:1;O2 and $[M + H- H_2O]^+$ of SM 41:2;O2. The accurate masses of $[M + H]^+$ and $[M + Na]^+$ of SM 38:1;O2 are 759.6374 and 781.6194 respectively. The $[M + Na]^+$ of SM 38:1;O2 has almost the same mass as $[M + H]^+$ of SM 40:4;O2 (m/z 781.6218) and thus, is the main interference of SM 40:4;O2 in the HRMS method (Fig. 3(A)). However, in the MRM method, SM 38:1;O2 will form a product ion of 206 which corresponds to the sodium phosphocholine headgroup instead of 184.07. The transitions of $[M + Na]^+$ of SM 38:1;O2 will be 781.6 → 206 instead of 781.6 → 184.07 and no correction is required in MRM method (Fig. 3(B)). Another source of interference could be $[M + H-H_2O]^+$ of SM 41:2;O2 which has the transition of 781.6582 → 184.07, accounting for 0.05% of the signal of $[M + H]^+$ of SM 41:2;O2. The ion type interference for all other lipid classes are specified in **Supplemental Table S8**.

The example of isotopic interference can be demonstrated by using sphingolipids classes such as Cer, LacCer, HexCer. These classes are dominated by the sphingoid backbone fragments 266, 264, 262 corresponding to the backbone d18:0, d18:1, d18:2 respectively [40]. These fragments can lead to interference, as the product ion of M + 2 of d18:2 can contribute to the response of d18:1. Likewise, M + 2 product ion of d18:1 can contribute to the response of d18:0. Hence, these kinds of interferences should be corrected.

The corresponding type II isotopic correction for all no/partially separated lipid features was performed by LICAR [35]. Criteria 6 was met for the features with non-zero concentration after isotopic and interfering adduct/ion type correction.

3.4 Report confidence

The scores are assigned based on the attainment of criteria as described in Fig. 1(B). For fully separated classes, features that at least meet the criteria 1 + 2 + 4 + 5 + 6 receive a score 4. For no/partially separated classes, score 4 is assigned to the features meeting at least the criteria 1 + 2 + 3 + 6. For no/partially separated classes, the features fulfilling criteria 1 + 2 + 5 + 6 are given a score of 3. All other features irrespective of no/partial/full separation, meeting criteria 1 + 2 + 6 are given score 2, while ones fulfilling criteria 1 + 2 get score 1. Depending on the fulfillment of criteria, each lipid feature has been given a score as shown in **Supplemental Table S5 (sheet 3)**.

Names are assigned to the highest confidence features with score 4. The features with scores 3 and 2 are considered putatively annotated, while the features with score 1 are designated as unknowns.

3.5 Validation in human K2 EDTA plasma

The in-house human K2 EDTA plasma was used as matrix and one-IS per class mix was used for assessing the performance of HILIC-MS/MS method. The calibration lines of IS spiked in pure solvent and in plasma (before and after extraction) are shown in **Fig. S2**. Linearity, LOD, LOQ, carryover, precision, recovery, ion suppression and matrix effect were assessed and reported in **Table 1 and Supplemental Table S5 (sheet 4)**.

The LODs and LOQs were as low as 0.60 pmol mL^{-1} and 1.31 pmol mL^{-1} respectively (except for CE) which makes our method sensitive enough to detect the lipids at low concentrations in 25 µL of plasma. The linear regression coefficients (R2) were above 0.98 for most of the lipid classes except for CE where it was 0.97. The carryover was analyzed in the blank samples placed right after the plasma samples (spiked with highest calibration point before extraction). Apart from PS and LPS, all the lipid classes showed a carryover of below 2%. The intra-day and inter-day precisions were determined at L, M and H concentration levels. Almost all the classes have RSD (%) below 15% except for DG, Cer and CE. The recovery was in the range of (53–112) % for most of the lipid classes but for the polar classes such as LPG, LPS and LPI, the recovery is poor which may reflect the current extraction method is less suited for polar lipids and these classes may need a dedicated extraction method.

Table 1. Summary of the validation parameters for human K2 EDTA plasma samples using one-IS per class mix.

Lipid class	Internal standards	linearity	LOD (nmol mL^{-1})	LOQ (nmol mL^{-1})	Intraday Precision (%)			Interday Precision (%)		
					low	medium	high	low	medium	high
Phosphatidylcholine	PC 15:0/18:1-d7	0.995	0.0306	0.071	2.69	2.43	3.13	7.09	9.16	8.72
Phosphatidylethanolamine	PE 15:0/18:1-d7	0.995	0.0006	0.0013	3.67	7.08	3.67	8.23	6.99	6.04
Phosphatidylserine	PS 15:0/18:1-d7	0.999	0.0014	0.0041	8.41	4.81	5.22	8.29	5.75	5.26
Phosphatidylglycerol	PG 15:0/18:1-d7	0.997	0.001	0.0024	0.75	1.83	1.79	7.34	3.47	3.46
Phosphatidylinositol	PI 15:0/18:1-d7	0.994	0.0051	0.016	5.87	4.48	1.88	4.56	5.78	3.17
Lysophosphatidylcholine	LPC 18:1-d7	0.992	0.0032	0.0089	0.36	1.02	2.4	4.97	5.57	6.76
Lysophosphatidylethanolamine	LPE 18:1-d7	0.992	0.0011	0.0021	2.14	1.43	5.49	7.13	6.83	6.79
Cholesteryl esters	CE 18:1-d7	0.970	2.0202	6.6603	16.89	10.76	7.82	12.87	13.01	19.99
Diglycerides	DG 15:0/18:1-d7	0.982	0.0495	0.129	2.44	8.29	8.32	15.89	33.26	29.25
Triglycerides	TG 15:0/18:1-d7/15:0	0.992	0.0086	0.0247	0.88	3.19	0.51	12.73	11.84	8.62
Sphingomyelin	SM 18:1;O2/18:1-d9	0.990	0.0013	0.0033	2.85	1.59	1.87	3.7	12.86	7.46
Lysophosphatidylglycerol	LPG 17:1	0.992	0.0011	0.0035	2.99	3.18	3.83	5.25	9.03	8.92
Lysophosphatidylinositol	LPI 17:1	0.992	0.0007	0.0021	3.52	2.04	5.87	14.16	13.67	14.91
Lysophosphatidylserine	LPS 17:1	0.991	0.0036	0.005	7.21	5.57	4.87	9.92	5.71	7.38
Ceramides	Cer 18:1;O2/16:0-d9	0.981	0.0241	0.0581	9.63	29.68	34.15	21.76	21.37	18.59
Ceramides	Cer 18:0;O2/16:0-d9	0.989	0.0057	0.008	2.91	0.57	2.22	4.51	5.65	7.21
Hexosylceramides	Hex-Cer 18:1;O2/16:0-d9	0.998	0.0053	0.0108	16.46	6.74	11.16	11.82	8.87	8.69
Lactosylceramides	Lac-Cer 18:1;O2/16:0-d9	0.993	0.0056	0.0119	9.78	12.96	4.98	15.34	14.29	23.51

It was observed that non-polar classes such as DG and CE show severe ion suppression and matrix effects as these classes elute at the same retention time as TG. The TG class has very high endogenous concentrations which may lead to the ion suppression of DG and CE. The polar classes such PC and LPC also show significant ion suppression that may be due to the interference from the matrix. LPG, LPI and LPS show severe matrix effects at L and M level concentration. In our HILIC method, the internal standards co-elute with the endogenous compounds, hence the issues related to poor recovery, severe ion suppression and matrix effects can be compensated by the use of appropriate internal standards.

The repeatability of our HILIC-MS/MS method was determined by measuring the RSD of endogenous lipid features in 12 QC samples. These QC samples were inserted at an interval of every 10 samples in the covid patient samples batch. It was found that 20 lipid features showed RSD below 5% while 360 and 380 lipid features showed RSD in between (5–10) % and (10–15) % respectively. 227 had RSD in the range of (15–20) % while 75 have RSD in between (20–30) %.

In total, 1062 endogenous lipid features show an RSD below 30% (**Fig. 5(A)**) which in accordance with the metabolomics study requirements.

3.6 Accurate quantitation in NIST SRM 1950 plasma

In NIST SRM 1950 plasma, 608 lipid species across 19 classes with score 4 were quantified. The quantitation strategies are listed in **Fig. 4 (A)**. The unavailability of commercial standards for all endogenous lipid species leads to limitations in achieving absolute quantitation, but HILIC has an advantage over other separation techniques as the elution of species occurs according to their head group, so all species in a particular class elute at almost the same time and have similar ionization efficiencies. Since we lack individual standards for each endogenous lipid species, we are using multiple internal standards per class to achieve quantitation as accurate as possible. Here, we further use the multi-ISs per class strategy to correct for the response factor to report measured lipid concentrations for the NIST SRM 1950 plasma.

Another factor to be taken into account is the different response of sn-1 and sn-2 of phospholipids in MRM experiments [41]. Determining ratios between fragment ions of

positional isomers can help determine the sn-positions of fatty acyl chains in glycerophospholipids [14]. Using this strategy, we defined the positional isomers of lipid species and then assigned internal standards for quantitation. The response of both fatty acyl chains at sn-1 and sn-2 position of phospholipid species were examined to determine the position of the chains. **Supplemental Table S9** illustrates the ratios of the sn-1/sn-2 carboxylate anion of phospholipids ISs at different collision energies. At collision energies of 30, 40, and 50 eV, the sn-1/sn-2 response ratios of PI and PS are above 1, whereas those of PC, PE, and PG are below 1. There is an exception where the ratio is more than 1 when the sn-2 chain is 22:4 at collision energy of 60 eV. Further, we determined the ratio of two transitions of fatty acid chains of endogenous species in the NIST plasma samples to identify the dominant isomers. We took sn-1/sn-2> 1 or sn-1/sn-2< 1 to define the dominant isomer.

After determining the sn-1 and sn-2 ratios, we used calibration lines using multi-ISs per class. The calibration lines with $R2 < 0.98$ were dropped, except for CE and DG with criteria of $R2 > 0.96$. The next step was to assign an IS based on total carbon number and double bond equivalents of endogenous compounds. If the total carbon number was same, then the double bond equivalents was also taken into account (**Supplemental Table S5, sheet 5**). The sn-1 and sn-2 information of endogenous metabolites was considered while assigning the ISs and post-hoc correction was used to correct for metabolites with two of the same fatty acyl chains, e.g. PC 18:1_18:1.

The TG classes with three fatty acyl chains are more complex and it is difficult to determine their fatty acyl chain position with our current method. Hence, their quantitation was performed considering only the total carbon number and double bond equivalents of the fatty acyl chains. The concentration values of the lipid species in the NIST plasma samples are specified in **Supplemental Table S5 (sheet 6)**. The correlation of the NIST SRM 1950 data with that from published consensus values [42,43,21] shows overall good correlation with R2 ranging from 0.64 to 0.84 (**Fig. 4(B)**).

Although we applied several strategies to achieve the accurate quantitation, our method is still limited due to the lack of a suitable model to correct the response factor for the sn-1/sn-2 isomer ratio and lack of (internal) standards for individual compounds.

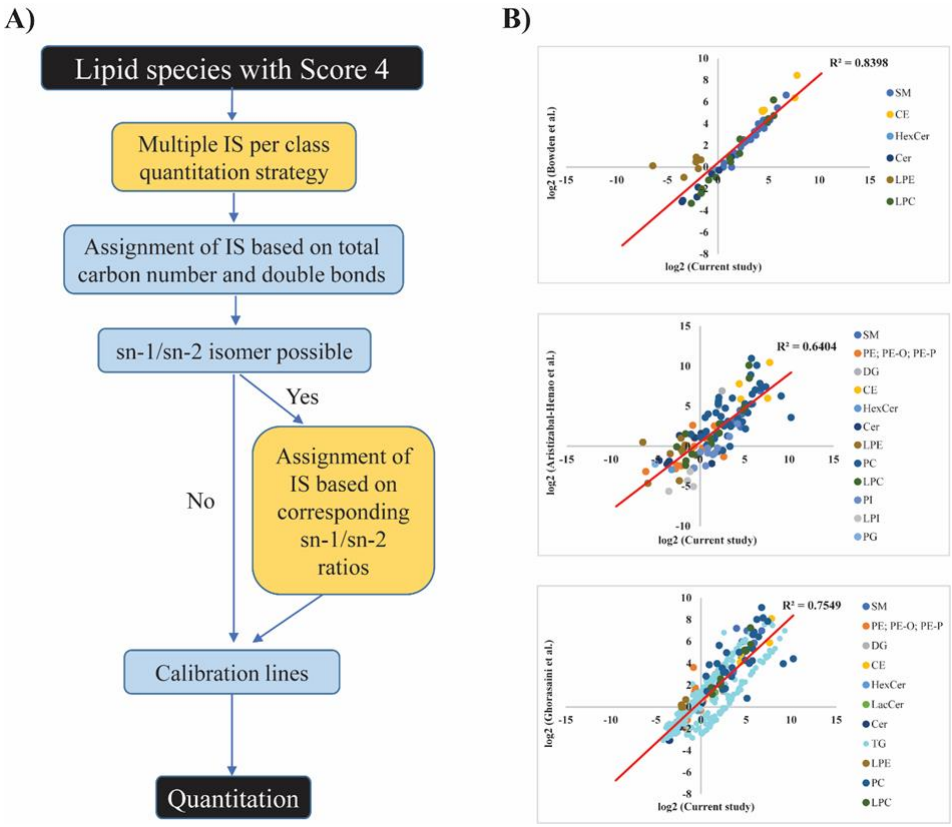

Fig. 4. A) Decision tree of lipids quantitation. B) Correlations of lipid concentrations (nmol mL-1, base 2 logarithm) between our HILIC-MS/MS method and reported literature values (a. Bowden et al, 2017; b. Aristizabal-Henao et al, 2020, c. Ghorasaini et.al, 2021).

3.7 Application of HILIC MS/MS lipidomics method in COVID-19 plasma samples

Next, we applied this method to discover plasma lipid biomarkers for COVID-19 severity using all the lipid features irrespective of their confidence scores. The plasma lipid extracts of 25 patients housed in the hospital ward and 78 patients in ICU were analyzed in a random order by this HILIC-MS/MS method. QC samples were inserted between every 10 study samples for data quality control and batch correction. After peak integration, 1062 lipid features with a QC RSD < 30% and with a distribution of the coefficient of variation (%) shown in **Fig. 5(A)** were selected for subsequent statistical analyses.

The PCA plot shows good separation between the ward and ICU patients (**Fig. 5(B)**), which indicates a widely changed lipidome in severe COVID-19 patients. A linear regression

model was used to find out the most important biomarker candidates distinguishing the patients in the ward from ICU. The modeling results showed that a total of 511 identified lipid features (score 2, 3&4) and 9 unknowns (score 1) across 18 lipid (sub)classes with FC $\geqslant$ 1.3 or FC $\leqslant$ 0.7 as well as false discovery rate (FDR) Q < 0.05 were significant (**Supplemental Table S5, sheet 7**). The volcano plot of these significantly changed lipid metabolites is shown in **Fig. 5(C)**. In general, Cers, glycerophospholipids, DGs, TGs, short chain SMs, and plasmalogen phosphoethanolamines were significantly increased, and six saturated/monounsaturated PIs, one LacCer, four SMs, one plasmalogen phosphoethanolamine (PE O-16:0/20:4) and two CEs were significantly ($\geqslant$30% median fold change, and Q < 0.05) decreased in ICU patients as compared to the those in the ward.

Specifically, TGs were identified as having higher abundance in the ICU patients compared with those in the ward. TGs are an important source of energy metabolism in the liver and many COVID-19 patients showed liver function abnormalities [8,44]. This is also supported by the lower total CE, which is often observed in liver damage [45].

Glycerophospholipids and sphingolipids are the major components of cell membranes and play a key role of maintaining the balance of the in vivo energy metabolism. Reports showed that phospholipids were significantly decreased in severe covid patients [7]. However, increased glycerophospholipid levels, including PC, PE, PI, PG, PS, and corresponding lysophospholipids were observed in our results. This may be because 80% of the patients of this cohort had chloroquine treatment, which has been reported to increase phospholipid levels [46].

Sphingolipids are also essential components of biomembrane lipid rafts which mediate signal transduction and immune activation processes. Critical patients are characterized by a decrease in SMs and elevated levels of Cers, HexCers. In severe patients, the altered lipidome of lipid rafts compositions may lead to cell apoptosis and immunoescape [10].

The application of our method in the COVID-19 plasma samples shows mainly class-based changes in the lipid profiles. There are also strong associations observed between severity of disease progression with fatty acid chain composition and saturation degree. Although a biological interpretation is not the aim of this paper, our results demonstrate that the HILIC-

MS/MS-based targeted lipidomics methodwith wide coverage is very promising for disease biomarker discovery.

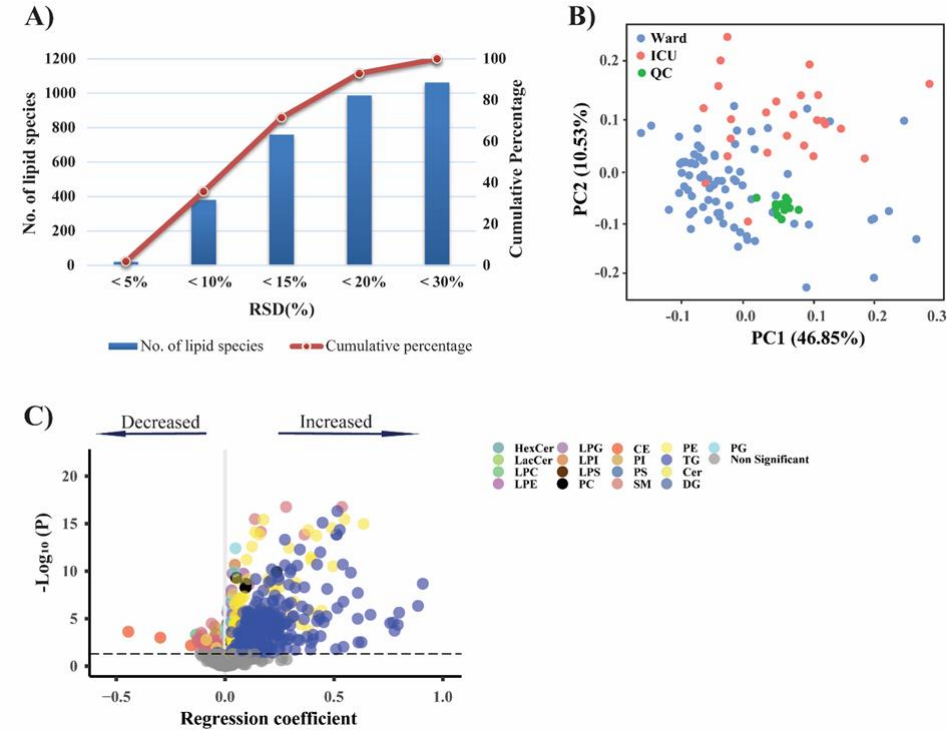

Fig. 5. Application in COVID-19 patients to distinguish the disease severity. A) Repeatability of lipid features in pooled QC samples of COVID-19 patients; B) PCA scores plot of samples from patients admitted to ward, or ICU and QCs, based on all metabolite data (cube-root transformed and Pareto-scaled); C) Volcano plot comparing plasma metabolites of patients in ICU with ward. Significantly altered metabolites with FDR < 0.05 are highlighted with different colors for different classes. Negative values indicate decreased and positive values indicate increased levels in ICU patients.

Conclusions

The lipidomics field is continuously evolving and a significant amount of work has been done in this area in recent years. But still two important aspects have been missing, comprehensive coverage spanning non-polar to polar lipid classes and quantifying the different lipid species at the fatty acyl chain level. To achieve this, it is crucial to follow the standardized workflow as proposed by Lipidomics Standards Initiative to avoid over-

reporting and false identification [29]. Herein, we describe a HILIC-MS/MS method with the initial target list of 1200 lipid features across 19 lipid (sub)classes. These lipid features were evaluated using various cross-class and within-class interference criteria for confirmation of their identification. Scores have been assigned to all these features showing the confidence in their identification. Further, we provided accurate quantitation of 608 lipid species with score 4 in NIST SRM plasma using multiple-ISs per class and a post-hoc correction strategy. This HILIC-MS/MS based lipidomics method was validated and was applied to COVID-19 patient samples. All detected features were used for biomarker discovery in COVID-19 plasma samples and features with high confidence were used for quantitation and comparison with other reported studies. Around 1062 detected lipid features from 25 µL of plasma were reported in COVID-19 patient plasma and dramatic class-based lipidome alterations indicated the changes in energy metabolism.

In conclusion, we have applied several strategies for high confidence lipid identification to avoid over-reporting of lipid species. This method has the competence of comprehensive lipidome coverage and can be used to extend the existing libraries of lipid features. Despite the fact that several strategies were applied to provide lipid concentrations at the fatty acyl chain level, limitations remain due to lack of a suitable model to correct for response factor for fatty acyl chain positional isomers. Nevertheless, this work has demonstrated potential in biomarker discovery to help in improving clinical lipidomics studies and will also encourage lipidomics researchers to use methods reporting lipids at a detailed structural level.

Acknowledgements

The authors would like to thank all the participants of this study for their time and effort.

Funding

This work was supported by the Dutch Research Council (NWO) ‘Investment Grant NWO Large’ program, for the ‘Building the infrastructure for Exposome research: Exposome-Scan’ [No. 175.2019.032]; the TKI-LSH project ‘METACOVID’ [No. LSHM20060]; the NWO Netherlands X-omics Initiative [No. 184.034.019]; METABODELTA: Metabolomics for clinical advances in the Medical Delta; MXL Fieldlab was funded by EFRO-grant

‘Kansen voor West II’ [No. KVW-00267]; the China Scholarship Council [No. 201608140084]; European Union’s Horizon 2020 Research and Innovation Program under the Marie Skłodowska-Curie grant agreement PoLiMeR [No. 812616].

References

1 M.R. Wenk. Lipidomics: new tools and applications, *Cell* 143 (2010) 888-895, https://doi.org/10.1016/j.cell.2010.11.033.

2 C.E. Stokes, J.N. Hawthorne, Reduced phosphoinositide concentrations in anterior temporal cortex of Alzheimer-diseased brains, *J. Neurochem.* 48 (1987) 1018–1021, https://doi.org/10.1111/j.1471-4159.1987.tb05619.x.

3 A. Mukherjee, Y. Ma, F. Yuan, Y. Gong, Z. Fang, E.M. Mohamed, E. Berrios, H. Shao, X. Fang, Lysophosphatidic acid up-regulates hexokinase II and glycolysis to promote proliferation of ovarian cancer cells, *Neoplasia* 17 (2015) 723–734, https://doi.org/10.1016/j.neo.2015.09.003.

4 R.W. Gross, X. Han, Lipidomics in diabetes and the metabolic syndrome. *Methods Enzymol*. 433 (2007) 73-90, https://doi.org/10.1016/S0076-6879(07) 33004-8.

5 P. G´erard, The crosstalk between the gut microbiota and lipids, *OCL* 27 (2020) 70, https://doi.org/10.1051/ocl/2020070.

6 B. Shen, X. Yi, Y. Sun, X. Bi, J. Du, C. Zhang, S. Quan, F. Zhang, R. Sun, L. Qian, W. Ge, W. Liu, S. Liang, H. Chen, Y. Zhang, J. Li, J. Xu, Z. He, B. Chen, J. Wang, H. Yan, Y. Zheng, D. Wang, J. Zhu, Z. Kong, Z. Kang, X. Liang, X. Ding, G. Ruan, N. Xiang, X. Cai, H. Gao, L. Li, S. Li, Q. Xiao, T. Lu, Y. Zhu, H. Liu, H. Chen, T. Guo, Proteomic and metabolomic characterization of COVID-19 patient sera, *Cell* 182 (2020) 59–72, https://doi.org/10.1016/j.cell.2020.05.032, e15.

7 M.A. Hussein, N.E.M. Ismail, A.H. Mohamed, R.M. Borik, A.A. Ali, Y.O. Mosaad, Plasma phospholipids: a promising simple biochemical parameter to evaluate COVID-19 infection severity, *Bioinform. Biol. Insights* 15 (2021), https://doi.org/10.1177/11779322211055891, 117793222110558.

8 D. Wu, T. Shu, X. Yang, J.-X. Song, M. Zhang, C. Yao, W. Liu, M. Huang, Y. Yu, Q. Yang, T. Zhu, J. Xu, J. Mu, Y. Wang, H. Wang, T. Tang, Y. Ren, Y. Wu, S.-H. Lin, Y. Qiu, D.-Y. Zhang, Y. Shang, X. Zhou, Plasma metabolomic and lipidomic alterations associated with COVID-19, *Natl. Sci. Rev.* 7 (2020) 1157–1168, https://doi.org/10.1093/nsr/nwaa086.

9 M Abdalla, N.E.M Ismail, ah mohamed, R.M. Borik, Aa ali, Y.O Mosaad, Plasma Levels of Phospholipids in Patients With COVID-19; A Promising Simple Biochemical Parameter to Evaluate the Disease Severity, *Research Square* (2020), https://doi.org/10.21203/rs.3.rs-57302/v1.

10 E. Torretta, M. Garziano, M. Poliseno, D. Capitanio, M. Biasin, T.A. Santantonio, M. Clerici, S.L. Caputo, D. Trabattoni, C. Gelfi, Severity of COVID-19 patients predicted by serum sphingolipids signature, *Int. J. Mol. Sci.* 22 (2021) 10198, https://doi.org/10.3390/ijms221910198.

11 M. Abu-Farha, T.A. Thanaraj, M.G. Qaddoumi, A. Hashem, J. Abubaker, F. Al- Mulla, The role of lipid metabolism in COVID-19 virus infection and as a drug target, Int. J. Mol. Sci. 21 (2020) 3544, https://doi.org/10.3390/ijms21103544.

12 J.-W. Song, S.M. Lam, X. Fan, W.-J. Cao, S.-Y. Wang, H. Tian, G.H. Chua, C. Zhang, F.-P. Meng, Z. Xu, J.-L. Fu, L. Huang, P. Xia, T. Yang, S. Zhang, B. Li, T.-J. Jiang, R. Wang, Z. Wang, M. Shi, J.-Y. Zhang, F.-S. Wang, G. Shui, Omics-driven systems interrogation of metabolic dysregulation in COVID-19 pathogenesis, *Cell Metab.* 32 (2020) 188–202, https://doi.org/10.1016/j.cmet.2020.06.016, e5.

13 J.F. Osuna-Ramos, H. Rend´on-Aguilar, L.A.D. Jesús-Gonz´alez, J.M. Reyes-Ruiz, A. M.

Espinoza-Ortega, L.A. Ochoa-Ramírez, A. Romero-Utrilla, E. Ríos-Burgue˜no, A. Soto-Almaral, J.J. Ríos-Tostado, J.G. Romero-Quintana, H. Ponce-Ramos, C.N. Farfan-Morales, R.M. del ´Angel, H. Barajas-Martínez, J. Rodríguez-Mill´an, J.S. Velarde-F´elix, Serum lipid profile changes and their clinical diagnostic significance in COVID-19 Mexican patients, *Infectious Diseases (except HIV/AIDS)*, 2020. http://medrxiv.org/lookup /doi/10.1101/2020.08.24. 20169789 (accessed September 25, 2022).

14 M. Holˇcapek, G. Liebisch, K. Ekroos, Lipidomic analysis, *Anal. Chem* 90 (2018) 4249–4257, https://doi.org/10.1021/acs.analchem.7b05395.

15 B. Buszewski, S. Noga, Hydrophilic interaction liquid chromatography (HILIC)-a powerful separation technique, *Anal. Bioanal. Chem.* 402 (2012) 231–247, https://doi.org/10.1007/s00216-011-5308-5.

16 E. Cífkov´a, M. Holˇcapek, M. Lísa, D. Vr´ana, B. Melichar, V. ˇStudent, Lipidomic differentiation between human kidney tumors and surrounding normal tissues using HILIC-HPLC/ESI–MS and multivariate data analysis, *J. Chromatogr. B* 1000 (2015) 14–21, https://doi.org/10.1016/j.jchromb.2015.07.011.

17 H.K. Kotapati, P.D. Bates, Normal phase HPLC method for combined separation of both polar and neutral lipid classes with application to lipid metabolic flux, *J. Chromatogr. B* 1145 (2020), 122099, https://doi.org/10.1016/j. jchromb.2020.122099.

18 P.D. Rainville, C.L. Stumpf, J.P. Shockcor, R.S. Plumb, J.K. Nicholson, Novel application of reversed-phase UPLC-oaTOF-MS for lipid analysis in complex biological mixtures: a new tool for lipidomics, *J. Proteome Res.* 6 (2007) 552–558, https://doi.org/10.1021/pr060611b.

19 C.G. Vasilopoulou, K. Sulek, A.D. Brunner, et al., Trapped ion mobility spectrometry and PASEF enable in-depth lipidomics from minimal sample amounts, *Nat. Commun.* 11 (2020) 331, https://doi.org/10.1038/s41467-019- 14044-x.

20 U. Loizides-Mangold, On the future of mass-spectrometry-based lipidomics, *FEBS J.*280 (2013) 2817–2829, https://doi.org/10.1111/febs.12202.

21 M. Ghorasaini, Y. Mohammed, J. Adamski, L. Bettcher, J.A. Bowden, M. Cabruja,K. Contrepois, M. Ellenberger, B. Gajera, M. Haid, D. Hornburg, C. Hunter, C. M. Jones, T. Klein, O. Mayboroda, M. Mirzaian, R. Moaddel, L. Ferrucci, J. Lovett, K. Nazir, M. Pearson, B.K. Ubhi, D. Raftery, F. Riols, R. Sayers, E.J.G. Sijbrands, M.P. Snyder, B. Su, V. Velagapudi, K.J. Williams, Y.B. de Rijke, M. Giera, Crosslaboratory standardization of preclinical lipidomics using differential mobility spectrometry and multiple reaction monitoring, *Anal. Chem.* 93 (2021) 16369–16378, https://doi.org/10.1021/acs.analchem.1c02826.

22 Z. Cao, T.C. Schmitt, V. Varma, D. Sloper, R.D. Beger, J. Sun, Evaluation of the performance of lipidyzer platform and its application in the lipidomics analysis in mouse heart and liver, *J. Proteome Res.* 19 (2020) 2742–2749, https://doi.org/10.1021/acs.jproteome.9b00289.

23 R. Lerner, D. Baker, C. Schwitter, S. Neuhaus, T. Hauptmann, J.M. Post, S. Kramer, L. Bindila, Four-dimensional trapped ion mobility spectrometry lipidomics for high throughput clinical profiling of human blood samples, *Nat. Commun.* 14 (2023) 937, https://doi.org/10.1038/s41467-023-36520-1.

24 J. Medina, R. Borreggine, T. Teav, L. Gao, S. Ji, J. Carrard, C. Jones, N. Blomberg, M. Jech, A. Atkins, C. Martins, A. Schmidt-Trucksass, M. Giera, A. Cazenave-Gassiot, H. Gallart-Ayala, J. Ivanisevic, Omic-scale high-throughput quantitative LC–MS/MS approach for circulatory lipid phenotyping in clinical research, *Anal. Chem.* 95 (2023) 3168–3179, https://doi.org/10.1021/acs.analchem.2c02598.

25 N.R. Zhang, N.G. Hatcher, K. Ekroos, K. Kedia, M. Kandebo, J.N. Marcus, S.M. Smith, K.P. Bateman, D.S. Spellman, Validation of a multiplexed and targeted lipidomics assay for accurate quantification of lipidomes, *J. Lipid Res.* 63 (2022), 100218, https://doi.org/10.1016/j.jlr.2022.100218.

26 H.C. K¨ofeler, T.O. Eichmann, R. Ahrends, J.A. Bowden, N. Danne-Rasche, E. A. Dennis, M. Fedorova, W.J. Griffiths, X. Han, J. Hartler, M. Holˇcapek, R. Jir´asko, J.P. Koelmel, C.S.

Ejsing, G. Liebisch, Z. Ni, V.B. O'Donnell, O. Quehenberger, D. Schwudke, A. Shevchenko, M.J.O. Wakelam, M.R. Wenk, D. Wolrab, K. Ekroos, Quality control requirements for the correct annotation of lipidomics data, *Nat. Commun.* 12 (2021) 4771, https://doi.org/10.1038/s41467-021-24984-y.

27 S.M. Lam, H. Tian, G. Shui, Lipidomics, en route to accurate quantitation, Biochim. Biophys. *Acta (BBA) - Mol. Cell Biol. Lipids* 1862 (2017) 752–761, https://doi.org/ 10.1016/j.bbalip.2017.02.008.

28 K. Yang, X. Han, Accurate quantification of lipid species by electrospray ionization mass spectrometry-meets a key challenge in lipidomics, *Metabolites.* 1 (2011) 21–40, https://doi.org/10.3390/metabo1010021.

29 G. Liebisch, R. Ahrends, M. Arita, M. Arita, J.A. Bowden, C.S. Ejsing, W.J. Griffiths, M. Holˇcapek, H. K¨ofeler, T.W. Mitchell, M.R. Wenk, K. Ekroos, Lipidomics standards initiative consortium, lipidomics needs more standardization, *Nat. Metab.* 1 (2019) 745–747, https://doi.org/10.1038/s42255-019-0094-z.

30 V.B. O'Donnell, G.A. FitzGerald, R.C. Murphy, G. Liebisch, E.A. Dennis, O. Quehenberger, S. Subramaniam, M.J.O. Wakelam, Steps toward minimal reporting standards for lipidomics mass spectrometry in biomedical research publications, *Circ. Genom. Precis. Med.* (2020) 13, https://doi.org/10.1161/CIRCGEN.120.003019.

31 N. Karu, A. Kindt, A.J. van Gammeren, A.A.M. Ermens, A.C. Harms, L. Portengen, R.C.H. Vermeulen, W.A. Dik, A.W. Langerak, V.H.J. van der Velden, T. Hankemeier, Severe COVID-19 is characterised by perturbations in plasma amines correlated with immune response markers, and linked to inflammation and oxidative stress, *Metabolites* 12 (2022) 618, https://doi.org/10.3390/ metabo12070618.

32 N. Karu, A. Kindt, L. Lamont, A.J. van Gammeren, A.A.M. Ermens, A.C. Harms, L. Portengen, R.C.H. Vermeulen, W.A. Dik, A.W. Langerak, V.H.J. van der Velden, T. Hankemeier, Plasma oxylipins and their precursors are strongly associated with COVID-19 severity and with immune response markers, *Metabolites* 12 (2022) 619, https://doi.org/10.3390/metabo12070619.

33 V. Matyash, G. Liebisch, T.V. Kurzchalia, A. Shevchenko, D. Schwudke, Lipid extraction by methyl-tert-butyl ether for high-throughput lipidomics, *J. Lipid Res.* 49 (2008) 1137–1146, https://doi.org/10.1194/jlr.D700041-JLR200.

34 C. Hu, J. van Dommelen, R. van der Heijden, G. Spijksma, T.H. Reijmers, M. Wang, E. Slee, X. Lu, G. Xu, J. van der Greef, T. Hankemeier, RPLC-ion-trap-FTMS method for lipid profiling of plasma: method validation and application to p53 mutant mouse model, *J. Proteome Res.* 7 (2008) 4982–4991, https://doi.org/10.1021/ pr800373m.

35 L. Gao, S. Ji, B. Burla, M.R. Wenk, F. Torta, A. Cazenave-Gassiot, LICAR: an application for isotopic correction of targeted lipidomic data acquired with classbased chromatographic separations using multiple reaction monitoring, *Anal. Chem.* 93 (2021) 3163–3171, https://doi.org/10.1021/acs.analchem.0c04565.

36 G. Liebisch, E. Fahy, J. Aoki, E.A. Dennis, T. Durand, C.S. Ejsing, M. Fedorova, I. Feussner, W.J. Griffiths, H. K¨ofeler, A.H. Merrill, R.C. Murphy, V.B. O'Donnell, O. Oskolkova, S. Subramaniam, M.J.O. Wakelam, F. Spener, Update on LIPID MAPS classification, nomenclature, and shorthand notation for MS-derived lipid structures, *J. Lipid Res.* 61 (2020) 1539–1555, https://doi.org/10.1194/jlr. S120001025.

37 R.M. Gathungu, P. Larrea, M.J. Sniatynski, V.R. Marur, J.A. Bowden, J.P. Koelmel, P. Starke-Reed, V.S. Hubbard, B.S. Kristal, Optimization of electrospray ionization source parameters for lipidomics to reduce misannotation of in-source fragments as precursor ions, *Anal. Chem.* 90 (2018) 13523–13532, https://doi.org/10.1021/ acs.analchem.8b03436.

38 A. Criscuolo, M. Zeller, M. Fedorova, Evaluation of lipid in-source fragmentation on different orbitrap-based mass spectrometers, *J. Am. Soc. Mass Spectrom.* 31.2 (2019) 463-466, https://doi.org/10.1021/jasms.9b00061.

39 O.L. Knittelfelder, B.P. Weberhofer, T.O. Eichmann, S.D. Kohlwein, G. N. Rechberger, A versatile ultra-high performance LC–MS method for lipid profiling, *J. Chromatogr. B* 951–952 (2014) 119–128, https://doi.org/10.1016/j. jchromb.2014.01.011.

40 A. Singh, M. Del Poeta, Sphingolipidomics: an important mechanistic tool for studying fungal pathogens, *Front. Microbiol.* 7 (2016), https://doi.org/10.3389/fmicb.2016.00501.

41 J. Pi, X. Wu, Y. Feng, Fragmentation patterns of five types of phospholipids by ultra-high-performance liquid chromatography electrospray ionization quadrupole time-of-flight tandem mass spectrometry, *Anal. Methods* 8 (2016) 1319–1332, https://doi.org/10.1039/C5AY00776C.

42 J.A. Bowden, A. Heckert, C.Z. Ulmer, C.M. Jones, J.P. Koelmel, L. Abdullah, L. Ahonen, Y. Alnouti, A.M. Armando, J.M. Asara, T. Bamba, J.R. Barr, J. Bergquist, C.H. Borchers, J. Brandsma, S.B. Breitkopf, T. Cajka, A. Cazenave-Gassiot, A. Checa, M.A. Cinel, R.A. Colas, S. Cremers, E.A. Dennis, J.E. Evans, A. Fauland, O. Fiehn, M.S. Gardner, T.J. Garrett, K.H. Gotlinger, J. Han, Y. Huang, A.H. Neo, T. Hy¨otyl¨ainen, Y. Izumi, H. Jiang, H. Jiang, J. Jiang, M. Kachman, R. Kiyonami, K. Klavins, C. Klose, H.C. K¨ofeler, J. Kolmert, T. Koal, G. Koster, Z. Kuklenyik, I. J. Kurland, M. Leadley, K. Lin, K.R. Maddipati, D. McDougall, P.J. Meikle, N. A. Mellett, C. Monnin, M.A. Moseley, R. Nandakumar, M. Oresic, R. Patterson, D. Peake, J.S. Pierce, M. Post, A.D. Postle, R. Pugh, Y. Qiu, O. Quehenberger, P. Ramrup, J. Rees, B. Rembiesa, D. Reynaud, M.R. Roth, S. Sales, K. Schuhmann, M.L. Schwartzman, C.N. Serhan, A. Shevchenko, S.E. Somerville, L.St. John-Williams, M.A. Surma, H. Takeda, R. Thakare, J.W. Thompson, F. Torta, A. Triebl, M. Tr¨otzmüller, S.J.K. Ubhayasekera, D. Vuckovic, J.M. Weir, R. Welti, M.R. Wenk, C.E. Wheelock, L. Yao, M. Yuan, X.H. Zhao, S. Zhou, Harmonizing lipidomics: NIST interlaboratory comparison exercise for lipidomics using SRM 1950–metabolites in frozen human plasma, *J. Lipid Res.* 58 (2017) 2275–2288, https://doi.org/10.1194/jlr.M079012.

43 J.J. Aristizabal-Henao, C.M. Jones, K.A. Lippa, J.A. Bowden, Nontargeted lipidomics of novel human plasma reference materials: hypertriglyceridemic, diabetic, and African–American, *Anal. Bioanal. Chem.* 412 (2020) 7373–7380, https://doi.org/10.1007/s00216-020-02910-3.

44 C. Zhang, L. Shi, F.-S. Wang, Liver injury in COVID-19: management and challenges, *Lancet Gastroenterol. Hepatol.* 5 (2020) 428–430, https://doi.org/10.1016/S2468-1253(20)30057-1.

45 B. Francesco, P. Daniele, F. Domenico, C. Giovanna, T. Giulia, A. Francesco, V. Francesco, D.B. Maria, Reduced lysosomal acid lipase activity: a new marker of liver disease severity across the clinical continuum of non-alcoholic fatty liver disease? *World J. Gastroenterol.* 25 (2019) 4172–4180, https://doi.org/10.3748/wjg.v25.i30.4172.

46 K.Y. Hostetler, M. Reasor, P.J. Yazaki, Chloroquine-induced phospholipid fatty liver. Measurement of drug and lipid concentrations in rat liver lysosomes, *J. Biol.Chem.* 260 (1985) 215–219, https://doi.org/10.1016/S0021-9258(18)89718-6.

SUPPLEMENTARY MATERIAL

Supplementary material associated with this article can be found, in the online version, at doi:10.1016/j.chroma.2023.464342.

Method validation calculations:

LOD and LOQ were calculated by using the equation S1 and equation S2 respectively.

$$LOD = \frac{3 \times SD_{area C_{low}} + area_{blank}}{\frac{area_{Clow}}{[C_{low}]}} \quad \text{(S1)}$$

$$LOQ = \frac{10 \times SD_{area C_{low}} + area_{blank}}{\frac{area_{Clow}}{[C_{low}]}} \quad \text{(S2)}$$

where $SD_{area C_{low}}$ represents the standard deviation of the lowest concentration with signal to noise ratio greater than 3(Clow), $area_{blank}$ are the peak area of the blank and $\frac{area_{Clow}}{[C_{low}]}$ represents the ratio between peak area and concentration at Clow [1].

Carryover is the presence of analytes in the blank samples after injection of high concentration standards [2]. The carryover is calculated by assessing the peak area of analytes in the blank solvents to the peak area of plasma sample analyzed before the blank. The precision is determined by calculating the RSD (%) three consecutive measurements of samples at L, M and H concentration level. The intraday precision is measured on the same day while inter-day precision is calculated from the samples measured on 3 different days. The precision can be calculated by equation S3.

$$RSD\ (\%) = \frac{Standard\ deviation}{Mean} \times\ 100 \quad \text{(S3)}$$

The recovery, ion suppression and matrix effects were calculated in L, M, H levels (prepared in triplicates). The recovery was calculated by comparing the response of samples spiked before and after extraction (equation S4).

$$Recovery(\%) = \frac{Response\ of\ IS\ in\ plasma\ before\ extraction}{Response\ of\ IS\ in\ plasma\ after\ extraction} \times 100 \quad \text{(S4)}$$

The ion suppression and matrix effects are common problems related to mass spectrometry measurements, in which response of the analyte may be suppressed or enhanced due to the presence of matrix or other components interfering with the ionization of compounds. The ion suppression and matrix effects were calculated from equation S5 and S6 respectively.

$$Ion\ suppression(\%) = \frac{Response\ of\ IS\ in\ plasma\ after\ extraction}{Response\ of\ IS\ in\ neat\ standards} \times 100 \quad \text{(S5)}$$

$$Matrix\ effect(\%) = \frac{Response\ of\ IS\ in\ plasma\ before\ extraction}{Response\ of\ IS\ in\ water\ before\ extraction} \times 100 \quad \text{(S6)}$$

1 T. van der Laan, A.-C. Dubbelman, K. Duisters, A. Kindt, A.C. Harms, T. Hankemeier, High-Throughput Fractionation Coupled to Mass Spectrometry for Improved Quantitation in Metabolomics, *Anal. Chem.* 92 (2020) 14330–14338. https://doi.org/10.1021/acs.analchem.0c01375.

2 D. Wolrab, M. Chocholoušková, R. Jirásko, O. Peterka, M. Holčapek, Validation of lipidomic analysis of human plasma and serum by supercritical fluid chromatography–mass spectrometry and hydrophilic interaction liquid chromatography–mass spectrometry, *Anal. Bioanal. Chem.* 412 (2020) 2375–2388. https://doi.org/10.1007/s00216-020-02473-3.

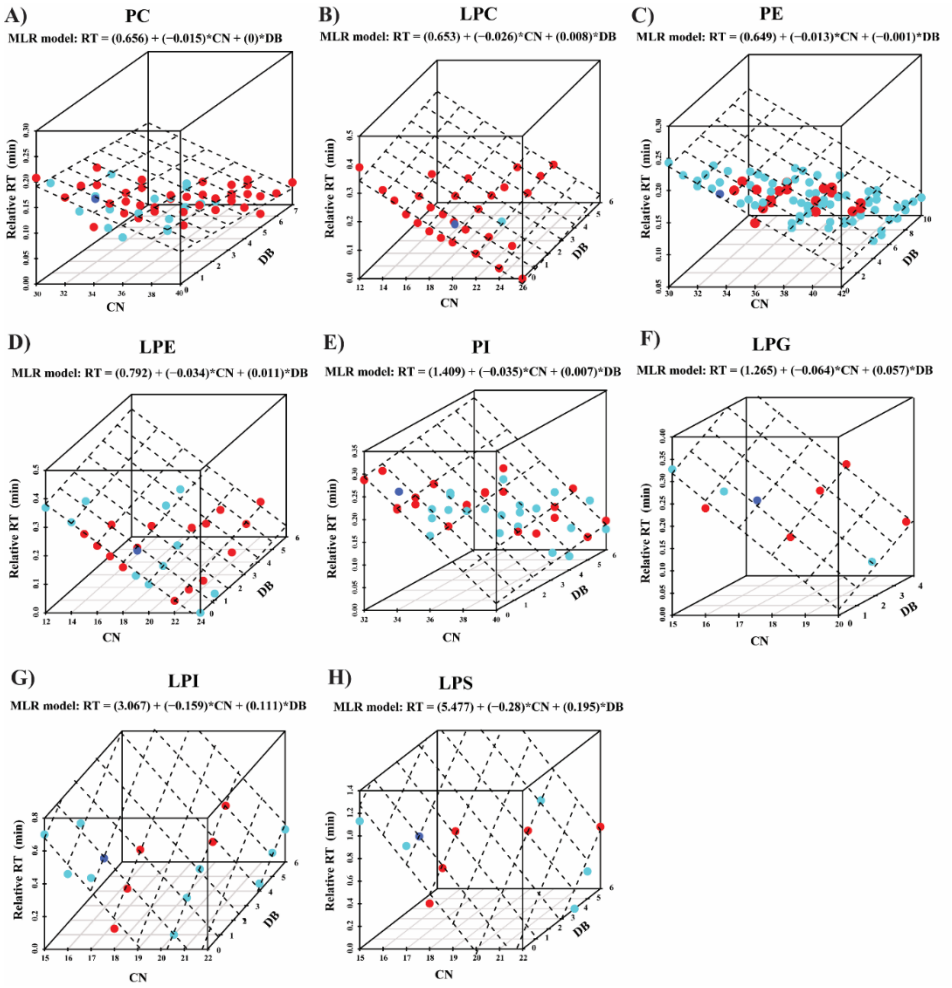

Figure S1. Multivariate linear regression analysis (MLR) of the relative retention time against the acyl chain carbon number (CN) and double bond number (DB) for each lipid features (red dots) within each lipid class depicted as 3D plot. A) PC; B) LPC; C) PE; D) LPE; E) PI; F) LPG; G) LPI; H) LPS. Lipids confirmed by RPLC-HRMS are colored in red, the remaining lipids fitting the retention time model with error rates less than 20% are colored in light blue and internal standards in dark blue.

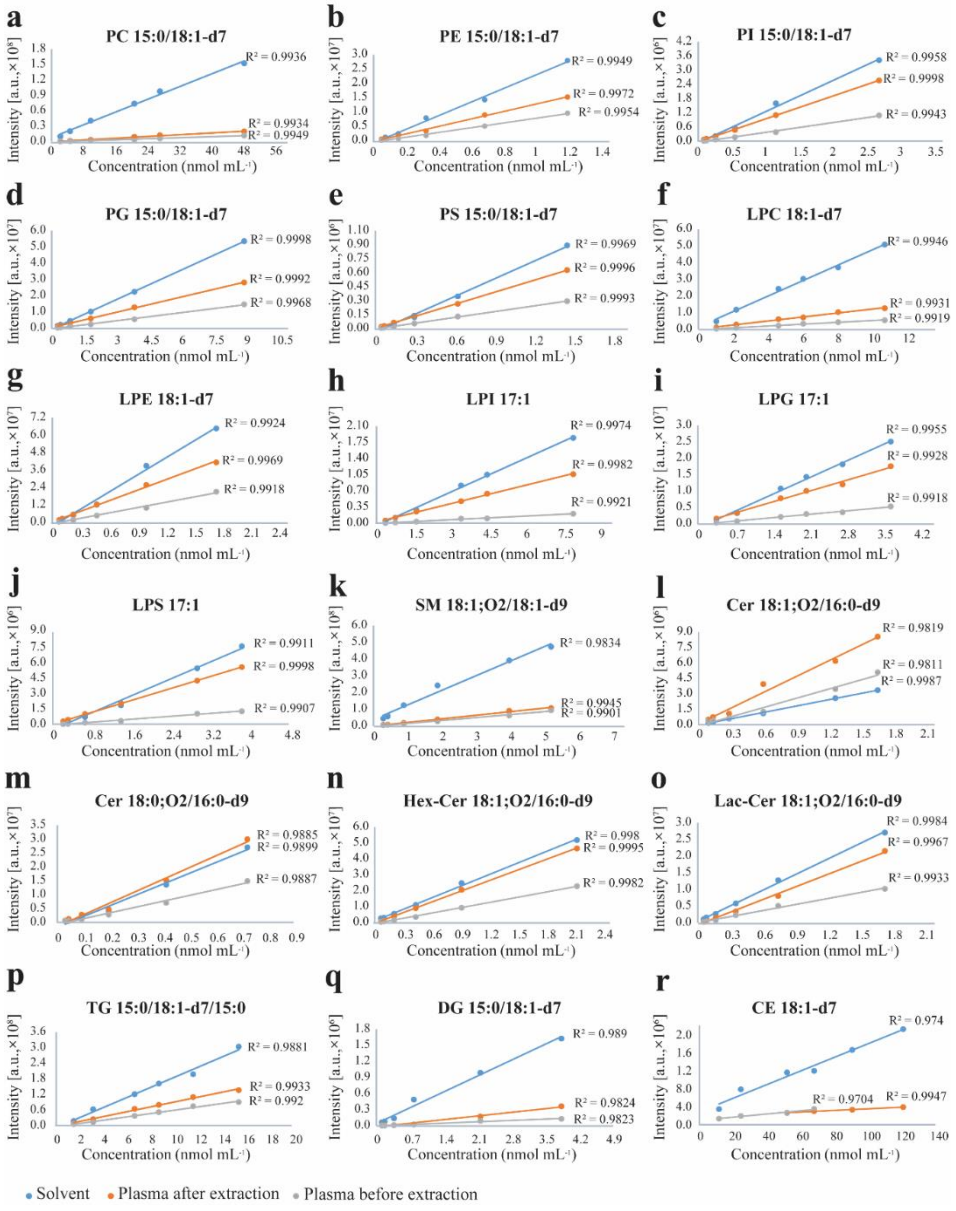

Figure S2. Calibration curves of deuterated or odd chain standards. a. PC 15:0/18:1-d7; b. PE 15:0/18:1-d7; c. PI 15:0/18:1-d7; d. PG 15:0/18:1-d7; e. PS 15:0/18:1-d7; f. LPC 18:1-d7; g. LPE 18:1-d7; h. LPI 17:1; i. LPG 17:1; j. LPS 17:1; k. SM 18:1;O2/18:1-d9; l. Cer 18:1;O2/16:0-d9; m. Cer 18:0;O2/16:0-d9, n. Hex-Cer 18:1;O2/16:0-d9; o. Lac-Cer 18:1;O2/16:0-d9; p. TG 15:0/18:1-d7/15:0; q. DG 15:0/18:1-d7; r. CE 18:1-d7. Calibration standards prepared in the pure solvent (blue), spiked in plasma after extraction (orange), and spiked in plasma before extraction (grey).

Table S1. The spiked concentration of lipid internal standard mixture in the COVID-19 plasma samples.

Internal standard	Source	Concentration (nmol mL^{-1})
TG 15:0/18:1-d7/15:0	SPLASH® LIPIDOMIX® Mass Spec Standard	8.55
CE 18:1-d7	SPLASH® LIPIDOMIX® Mass Spec Standard	65.80
SM 18:1;O2/18:1-d9	SPLASH® LIPIDOMIX® Mass Spec Standard	5.28
PC 15:0/18:1-d7	SPLASH® LIPIDOMIX® Mass Spec Standard	26.31
PE 15:0/18:1-d7	SPLASH® LIPIDOMIX® Mass Spec Standard	0.98
PG 15:0/18:1-d7	SPLASH® LIPIDOMIX® Mass Spec Standard	4.60
PS 15:0/18:1-d7	SPLASH® LIPIDOMIX® Mass Spec Standard	0.66
DG 15:0/18:1-d7	SPLASH® LIPIDOMIX® Mass Spec Standard	1.97
PI 15:0/18:1-d7	SPLASH® LIPIDOMIX® Mass Spec Standard	1.32
LPI 17:1	odd chain single standard	3.39
LPS 17:1	odd chain single standard	3.29
LPG 17:1	odd chain single standard	1.31
LPC 18:1-d7	SPLASH® LIPIDOMIX® Mass Spec Standard	5.92
LPE 18:1-d7	SPLASH® LIPIDOMIX® Mass Spec Standard	1.32
Cer 18:0;O2/16:0-d9	Lipidyzer®	0.96
Hex-Cer 18:1;O2/16:0-d9	Lipidyzer®	0.56
Lac-Cer 18:1;O2/16:0-d9	Lipidyzer®	0.75
Cer 18:1;O2/16:0-d9	Lipidyzer®	0.96

Table S2. Internal standard lipid mixture made of UltimateSPLASH™ ONE and SPLASH® LIPIDOMIX® with the insertion of additional standards for accurate quantitation.

Class	Internal standard	Source	mol wt.	Concentration (nmol mL^{-1})
TG	TG-d5 14:0/13:0/14:0	UltimateSPLASH™ ONE	714.18	10.50
	TG-d5 14:0/15:1/14:0	UltimateSPLASH™ ONE	740.22	20.26
	TG-d5 14:0/17:1/14:0	UltimateSPLASH™ ONE	768.27	29.29
	TG-d5 16:0/15:1/16:0	UltimateSPLASH™ ONE	796.33	37.67
	TG-d5 16:0/17:1/16:0	UltimateSPLASH™ ONE	824.38	45.49
	TG-d5 16:0/19:2/16:0	UltimateSPLASH™ ONE	850.42	35.28
	TG-d5 18:1/17:1/18:1	UltimateSPLASH™ ONE	876.46	25.67
	TG-d5 18:1/19:2/18:1	UltimateSPLASH™ ONE	902.47	16.62
	TG-d5 18:1/21:2/18:1	UltimateSPLASH™ ONE	930.53	8.06
	TG 15:0/18:1-d7/15:0	SPLASH® LIPIDOMIX® Mass Spec Standard	812.35	20.31
CE	CE-d7 14:1	UltimateSPLASH™ ONE	602.04	12.46
	CE-d7 16:1	UltimateSPLASH™ ONE	630.09	23.81
	CE-d7 18:1	UltimateSPLASH™ ONE	658.14	34.19
	CE-d7 20:3	UltimateSPLASH™ ONE	682.16	21.99
	CE-d7 22:4	UltimateSPLASH™ ONE	708.2	10.59
	CE 18:1-d7	SPLASH® LIPIDOMIX® Mass Spec Standard	658.14	159.54
	Cer 18:1;O2-d7/16:1	UltimateSPLASH™ ONE	542.93	41.44
	Cer 18:1;O2-d7/18:1	UltimateSPLASH™ ONE	570.98	26.27
	Cer 18:1;O2-d7/20:1	UltimateSPLASH™ ONE	599.03	12.52
Cer	Cer 18:1;O2-d7/22:1	UltimateSPLASH™ ONE	627.09	23.92
	Cer 18:1;O2-d7/24:1	UltimateSPLASH™ ONE	655.14	34.34
	Cer 18:1;O2/16:0-d9	Lipidyzer®	546.97	3.90
	Cer 18:0;O2/16:0-d9	Lipidyzer®	548.99	1.28
SM	SM-d9 18:1;O2/16:1	UltimateSPLASH™ ONE	710.08	31.69
	SM-d9 18:1;O2/18:1	UltimateSPLASH™ ONE	738.14	20.32
	SM-d9 18:1;O2/20:1	UltimateSPLASH™ ONE	766.19	9.79
	SM-d9 18:1;O2/22:1	UltimateSPLASH™ ONE	794.24	18.89
	SM-d9 18:1;O2/24:1	UltimateSPLASH™ ONE	822.28	27.36
	SM 18:1;O2/18:1-d9	SPLASH® LIPIDOMIX® Mass Spec Standard	738.12	12.19
PC	PC-d5 17:0/14:1	UltimateSPLASH™ ONE	723.04	20.75
	PC-d5 17:0/16:1	UltimateSPLASH™ ONE	751.09	39.94
	PC-d5 17:0/18:1	UltimateSPLASH™ ONE	779.15	57.76
	PC-d5 17:0/20:3	UltimateSPLASH™ ONE	803.17	37.35
	PC-d5 17:0/22:4	UltimateSPLASH™ ONE	829.21	18.09

	PC 15:0/18:1-d7	SPLASH® LIPIDOMIX® Mass Spec Standard	753.09	63.74
PE	PE-d5 17:0/14:1	UltimateSPLASH™ ONE	680.96	11.01
	PE-d5 17:0/16:1	UltimateSPLASH™ ONE	709.01	21.16
	PE-d5 17:0/18:1	UltimateSPLASH™ ONE	737.07	30.53
	PE-d5 17:0/20:3	UltimateSPLASH™ ONE	761.09	19.71
	PE-d5 17:0/22:4	UltimateSPLASH™ ONE	787.13	9.53
	PE 15:0/18:1-d7	SPLASH® LIPIDOMIX® Mass Spec Standard	711.01	2.11
PG	PG-d5 17:0/14:1	UltimateSPLASH™ ONE	733.95	10.22
	PG-d5 17:0/16:1	UltimateSPLASH™ ONE	762.01	19.68
	PG-d5 17:0/18:1	UltimateSPLASH™ ONE	790.06	28.48
	PG-d5 17:0/20:3	UltimateSPLASH™ ONE	814.08	18.43
	PG-d5 17:0/22:4	UltimateSPLASH™ ONE	840.12	8.93
	PG 15:0/18:1-d7	SPLASH® LIPIDOMIX® Mass Spec Standard	764.01	11.78
PS	PS-d5 17:0/14:1	UltimateSPLASH™ ONE	746.95	10.04
	PS-d5 17:0/16:1	UltimateSPLASH™ ONE	775	19.35
	PS-d5 17:0/18:1	UltimateSPLASH™ ONE	803.06	28.02
	PS-d5 17:0/20:3	UltimateSPLASH™ ONE	827.08	18.14
	PS-d5 17:0/22:4	UltimateSPLASH™ ONE	853.12	8.79
	PS 15:0/18:1-d7	SPLASH® LIPIDOMIX® Mass Spec Standard	777	1.93
DG	DG-d5 17:0/14:1	UltimateSPLASH™ ONE	557.91	13.44
	DG-d5 17:0/16:1	UltimateSPLASH™ ONE	585.97	25.60
	DG-d5 17:0/18:1	UltimateSPLASH™ ONE	614.02	36.64
	DG-d5 17:0/20:3	UltimateSPLASH™ ONE	638.04	23.51
	DG-d5 17:0/22:4	UltimateSPLASH™ ONE	664.08	11.29
	DG 15:0/18:1-d7	SPLASH® LIPIDOMIX® Mass Spec Standard	587.97	5.10
PI	PI-d5 17:0/14:1	UltimateSPLASH™ ONE	817.06	9.18
	PI-d5 17:0/16:1	UltimateSPLASH™ ONE	845.12	17.75
	PI-d5 17:0/18:1	UltimateSPLASH™ ONE	873.17	25.77
	PI-d5 17:0/20:3	UltimateSPLASH™ ONE	897.19	16.72
	PI-d5 17:0/22:4	UltimateSPLASH™ ONE	923.23	8.12
	PI 15:0/18:1-d7	SPLASH® LIPIDOMIX® Mass Spec Standard	847.12	3.54
LPI	LPI-d5 15:0	UltimateSPLASH™ ONE	580.66	12.92
	LPI-d5 17:0	UltimateSPLASH™ ONE	608.72	24.64
	LPI-d5 19:0	UltimateSPLASH™ ONE	636.77	11.78
	LPI 17:1	odd chain single standard	601.66	17.38
LPS	LPS-d5 15:0	UltimateSPLASH™ ONE	510.55	14.69
	LPS-d5 17:0	UltimateSPLASH™ ONE	538.61	27.85
	LPS-d5 19:0	UltimateSPLASH™ ONE	566.66	13.24

	LPS 17:1	odd chain single standard	531.55	18.81
LPG	LPG-d5 15:0	UltimateSPLASH™ ONE	497.55	15.07
	LPG-d5 17:0	UltimateSPLASH™ ONE	525.61	28.54
	LPG-d5 19:0	UltimateSPLASH™ ONE	553.66	13.55
	LPG 17:1	odd chain single standard	518.55	9.32
	LPC-d5 15:0	UltimateSPLASH™ ONE	486.63	15.41
LPC	LPC-d5 17:0	UltimateSPLASH™ ONE	514.7	29.14
	LPC-d5 19:0	UltimateSPLASH™ ONE	542.75	13.82
	LPC 18:1-d7	SPLASH® LIPIDOMIX® Mass Spec Standard	528.71	14.19
LPE	LPE-d5 15:0	UltimateSPLASH™ ONE	444.55	16.87
	LPE-d5 17:0	UltimateSPLASH™ ONE	472.61	31.74
	LPE-d5 19:0	UltimateSPLASH™ ONE	500.67	14.98
	LPE 18:1-d7	SPLASH® LIPIDOMIX® Mass Spec Standard	486.63	3.08
HexCer	Hex-Cer 18:1;O2/16:0-d9	Lipidyzer®	709.11	2.82
LacCer	Lac-Cer 18:1;O2/16:0-d9	Lipidyzer®	871.25	2.30

Table S3. Demographics of the COVID-19 patients in the lipidomics study. Values are n (%) or median [full range].

	Patients (n=44)	**Samples (n=103)**
Age, years	73 [49-87]	71 [49-87]
Male (%)	30 (68%)	65 (63%)
BMI	27 [19-42]	27 [19-42]
Admitted to ward	37 (84%)	78 (76%)
Admitted to ICU	7 (16%)	25 (24%)
Deceased	9 (20%)	
post-admission chloroquine	35 (80%)	

Table S4.

A. LC gradient table showing parameters for HILIC-MS/MS chromatographic separation of lipid classes.

Time (min)	Flow rate (mL/min)	Mobile Phase A (%)	Mobile Phase B (%)
0.00	0.2	100	0
2.00	0.2	100	0
2.10	1.0	100	0
11.00	1.0	50	50
11.50	1.0	30	70
12.50	1.0	30	70
12.60	0.2	100	0
14.00	0.2	100	0

B. LC gradient table showing parameters for RPLC-HRMS chromatographic separation of lipid classes.

Time (min)	Flow rate (mL/min)	Mobile Phase A (%)	Mobile Phase B (%)
0.00	0.4	50	50
0.50	0.4	50	50
10.00	0.4	3	97
13.00	0.4	3	97
13.10	0.4	50	50
16.00	0.4	50	50

Table S5. In supplemental excel.

Sheet 1. The first acquisition method including 602 transitions in switch polarity mode. The internal standards are highlighted in yellow.
Sheet 2. The second acquisition method including 598 transitions in switch polarity mode. The internal standards are highlighted in yellow.
Sheet 3. Report confidence scores of lipid features and corresponding lipid identifiers. "✓" represents the corresponding lipid feature fulfill the corresponding criteria; * represents the fatty acyl chain information is confirmed by the IDA.
Sheet 4. Summary of the validation parameters for human K2 EDTA plasma samples using one-IS per class mix.
Sheet 5. Parameters of the multi-internal standards (ISs) per class mix standards used for accurate quantitation.
Sheet 6. Quantitation results for NIST SRM 1950 plasma samples using multi-ISs per class mix.
Sheet 7. Significantly changed metabolites with FDR<0.05 in COVID-19 plasma samples of ICU patients compared to ward patients.

Table S6. Concentrations of the standard mix used in making the calibration curves for validation.

Standard (nmol mL^{-1})	cal-1	cal-2	cal-3	cal-4	cal-5	cal-6	cal-7	cal-8
PC 15:0/18:1-d7	1.48	2.18	4.61	9.77	20.69	27.09	36.12	48.16
PE 15:0/18:1-d7	0.05	0.07	0.15	0.32	0.68	0.90	1.20	1.59
PS 15:0/18:1-d7	0.04	0.07	0.14	0.30	0.63	0.82	1.09	1.46
PG 15:0/18:1-d7	0.27	0.40	0.85	1.81	3.82	5.01	6.68	8.90
PI 15:0/18:1-d7	0.08	0.12	0.26	0.54	1.15	1.51	2.01	2.68
LPC 18:1-d7	0.33	0.48	1.03	2.17	4.61	6.03	8.04	10.72
LPE 18:1-d7	0.07	0.11	0.22	0.47	1.00	1.31	1.75	2.33
CE 18:1-d7	3.71	5.45	11.55	24.46	51.80	67.80	90.41	120.54
DG 15:0/18:1-d7	0.12	0.17	0.37	0.78	1.66	2.17	2.89	3.86
TG 15:0/18:1-d7/15:0	0.47	0.69	1.47	3.11	6.59	8.63	11.51	15.35
SM 18:1;O2/18:1-d9	0.28	0.42	0.88	1.87	3.96	5.18	6.91	9.21
LPG 17:1	0.11	0.17	0.35	0.74	1.57	2.05	2.74	3.65
LPI 17:1	0.24	0.36	0.76	1.60	3.39	4.44	5.92	7.90
LPS 17:1	0.21	0.31	0.65	1.38	2.92	3.83	5.10	6.80
Cer 18:1;O2/16:0-d9	0.09	0.13	0.28	0.60	1.27	1.66	2.21	2.95
Cer 18:0;O2/16:0-d9	0.03	0.04	0.09	0.20	0.41	0.54	0.72	0.96
Hex-Cer 18:1;O2/16:0-d9	0.07	0.10	0.20	0.43	0.92	1.20	1.60	2.13
Lac-Cer 18:1;O2/16:0-d9	0.05	0.08	0.17	0.35	0.75	0.98	1.30	1.73

Table S7. Estimated error for the retention time model with carbon and unsaturated bond combination.

Class	Retention time range (min)	Adjusted R^2	Error rates
PE	0.24	0.94	7.80%
PC	0.21	0.89	17.92%
PI	0.29	0.93	11.97%
PS	0.23	0.93	23.94%
LPE	0.37	0.95	14.05%
LPC	0.39	0.95	10.53%
LPI	0.7	0.96	13.54%
LPG	0.33	0.93	9.79%
LPS	1.13	0.91	15.20%
SM	0.31	0.97	11.92%

Table S8. Transitions of interference from different ion types within the class and their average relative abundances in positive/negative-ion ESI MS/MS mass spectra of IS.

IS	Elemental formula	Observed ion	MS/MS		Relative abundance [%]
			Q1	Q3	
PC 15:0/18:1-d7	C41H73D7NO8P	$[M-H]^-$	751.6	288.3	n/a
		[M+OAc]-	811.6	288.3	100
		$[M+Cl]^-$	787.6	288.3	306
		$[M-15]^-$	737.6	288.3	28
PE 15:0/18:1-d7	C38H67D7NO8P	[M-H]-	709.6	288.3	100
PS 15:0/18:1-d7	C39H66D7NNaO10P	[M-H]-	752.5	288.3	100
PG 15:0/18:1-d7	C39H67D7NaO10P	[M-H]-	739.5	288.3	100
PI 15:0/18:1-d7	C42H75D7NO13P	[M-H]-	845.6	288.3	100
LPC 18:1-d7	C26H45D7NO7P	[M-H]-	527.4	288.3	n/a
		[M+OAc]-	587.4	288.3	100
LPE 18:1-d7	C23H39D7NO7P	[M-H]-	485.3	288.3	100
LPG 17:1	C23H45O9P	[M-H]-	495.3	267.4	100
LPI 17:1	C26H49O12P	[M-H]-	583.4	267.4	100
LPS 17:1	C23H44NO9P	[M-H]-	508.3	267.4	100
CE 18:1-d7	C45H71D7O2	[M+H]+	658.7	369.4	3.4
		[M+Na]+	680.6	369.4	n/a
		[M+NH4]+	675.7	369.4	100
DG 15:0/18:1-d7	C36H61D7O5	[M+H]+	588.6	346.3	22.84
		[M+NH4]+	605.6	346.3	100
		[M+Na]+	610.5	346.3	n/a
		[M+K]+	626.5	346.3	n/a
TG 15:0/18:1-d7/15:0	C51H89D7O6	[M+H]+	812.8	570.5	0.32
		[M+NH4]+	829.8	570.5	100
SM 18:1;O2/18:1-d9	C41H72D9N2O6P	[M+H]+	738.6	184.1	100
		[M+Na]+	760.6	184.1	n/a
		[M+K]+	776.6	184.1	n/a
		[M+NH4]+	755.7	184.1	0.05
		$[M+H-H_2O]+$	720.6	184.1	0.06
Cer 18:0;O2/16:0-d9	C34H60D9NO3	[M+H]+	549.6	266.4	100
		[M+Na]+	571.6	266.4	n/a
		[M+H-H2O]+	531.6	266.4	2647.6
		[M+H-2H2O]+	513.6	266.4	323.6
Cer 18:1;O2/16:0-d9	C34H58D9NO4	[M+H]+	547.6	264.4	100
		[M+Na]+	569.6	264.4	n/a
		[M+H-H2O]+	529.6	264.4	3583.3
		[M+H-2H2O]+	511.6	264.4	435.82
Hex-Cer 18:1;O2/16:0-d9	C40H68D9NO8	[M+H]+	709.6	264.4	100
		[M+Na]+	731.6	264.4	n/a
		[M+K]+	747.6	264.4	n/a

		[M+H-H2O]+	691.6	264.4	414.35
		[M+H-Hex]+	529.6	264.4	143.61
Lac-Cer 18:1;O2/16:0-d9	C46H78D9NO13	[M+H]+	871.7	264.4	100
		[M+Na]+	893.7	264.4	n/a
		[M+K]+	909.6	264.4	n/a
		[M+H-H2O]+	853.7	264.4	112.73

*100% represents the main peak used for the method construction. Percentage was calculated by the intensity of interference of other ion type or isotope divided by the main ion form for method construction.
n/a means below the LOD

Table S9. The sn-1/sn-2 ratios of fatty acyl tails of five phospholipid classes at different collision energies (30 eV, 40 eV, 50 eV and 60 eV) in ESI (−) mode.

Lipid class	ESI mode	sn-1/sn-2, (Collision Energy, eV)			
		30	40	50	60
PC 15:0/18:1-d7	(-)	0.36	0.37	0.36	0.35
PC-d5 17:0/14:1	(-)	0.41	0.39	0.50	0.69
PC-d5 17:0/16:1	(-)	0.51	0.46	0.49	0.57
PC-d5 17:0/18:1	(-)	0.96	0.82	0.80	0.80
PC-d5 17:0/20:3	(-)	0.79	0.78	0.71	0.84
PC-d5 17:0/22:4	(-)	0.87	0.88	0.85	1.24
PE 15:0/18:1-d7	(-)	0.39	0.43	0.46	0.37
PE-d5 17:0/14:1	(-)	0.35	0.38	0.50	0.67
PE-d5 17:0/16:1	(-)	0.36	0.37	0.42	0.53
PE-d5 17:0/18:1	(-)	0.39	0.40	0.43	0.46
PE-d5 17:0/20:3	(-)	0.44	0.44	0.54	0.75
PE-d5 17:0/22:4	(-)	0.54	0.54	0.75	1.40
PI 15:0/18:1-d7	(-)	2.53	2.84	1.93	1.42
PI-d5 17:0/14:1	(-)	1.44	1.17	1.21	1.27
PI-d5 17:0/16:1	(-)	1.41	1.18	1.11	1.10
PI-d5 17:0/18:1	(-)	1.26	1.17	1.06	1.04
PI-d5 17:0/20:3	(-)	1.27	1.04	1.08	1.22
PI-d5 17:0/22:4	(-)	1.49	1.10	1.15	1.52
PS 15:0/18:1-d7	(-)	1.75	2.20	2.82	2.78
PS-d5 17:0/14:1	(-)	1.97	2.19	2.80	3.60
PS-d5 17:0/16:1	(-)	2.10	2.20	2.54	2.94
PS-d5 17:0/18:1	(-)	1.99	2.04	2.39	2.67
PS-d5 17:0/20:3	(-)	1.95	2.04	2.91	3.54
PS-d5 17:0/22:4	(-)	2.50	2.52	3.62	5.36
PG 15:0/18:1-d7	(-)	0.44	0.43	0.39	0.37
PG-d5 17:0/14:1	(-)	0.46	0.45	0.52	0.66
PG-d5 17:0/16:1	(-)	0.49	0.43	0.43	0.51
PG-d5 17:0/18:1	(-)	0.50	0.46	0.44	0.46
PG-d5 17:0/20:3	(-)	0.50	0.49	0.51	0.66
PG-d5 17:0/22:4	(-)	0.48	0.60	0.69	1.11